The Properties of Single Crystal Sapphire Fibers and The Polarimetric Optical Sensor for High Temperature Measurements

by

Pinyi Zhang

Thesis submitted to the Faculty of the
Virginia Polytechnic Institute and State University
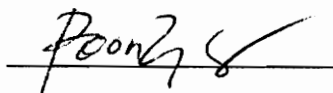in partial fulfillment of the requirements for the degree of

MASTER OF SCIENCE

in

Electrical Engineering

APPROVED:

Richard O. Claus

Richard O. Claus, Chairman

Poon

Ting-Chung Poon

Kent A. Murphy

Kent A. Murphy

February, 1994

Blacksburg, Virginia

The Properties of Birefringent Single Crystal Sapphire Fibers and Polarimetric Optical Sensors for High Temperature Measurements

by

Pinyi Zhang

Richard O. Claus, Chairman

Electrical Engineering

(ABSTRACT)

The polarization-maintaining properties of single crystal sapphire fibers are investigated and a polarimetric optical sensor for high temperature measurements is designed. The polarization-maintaining properties of single crystal sapphire fibers are investigated experimentally for different modal power distributions and different fiber lengths. Experimental results indicate that linearly polarized light launched along one of the principal axes of the birefringence can be partially maintained. The polarization-maintaining ability (PMA) has been measured to be 6 dB and 3 dB for 7 cm and 32 cm long sapphire fibers, respectively. The temperature coefficient of the differential phase delay between the orthogonal polarization modes has been measured to be 0.0208 rad / $^{\circ}$C m. A resolution of 2 $^{\circ}$C has been obtained over the measurement range of 25 $^{\circ}$C to 800 $^{\circ}$C. It is also observed that the PMA is strongly dependent on the mode-coupling parameter. The design of the polarimetric sapphire fiber sensor for high temperature measurements is based on the properties of withstanding high temperatures, polarization preservation and temperature dependence of phase delay. Since the temperature dependence of phase delay is proportional to the fiber length, consideration of a similar strain sensor is expected in the near future.

Acknowledgements

I would like to express my sincere gratitude to Dr. Richard O. Claus for his kind encouragement and guidance, for offering me the opportunity to work at FEORC, serving as my academic advisor and as the Chairman of the graduate committee. I would also like to thank Dr. Ting C. Poon and Dr. Kent A. Murphy for serving as committee members and for their great help.

I must thank Dr. A. B. Wang and Dr. Kent A. Murphy for their patient teaching, timely support and constant guidance on my experiment. I have learned much from them through working with them. Special appreciation goes to Russell May, Mike Gunther and Dr. V. S. Sudarshanam for their great help and assistance. I also thank other members of FEORC for their friendly help at all times.

I wish to express my sincere gratitude and appreciation to my husband and daughter for their love, help and support in all my academic endeavors. I also thank my parents, sisters and brothers in China for encouraging me in my academic studying.

Table of Contents

List of Figures

List of Tables

Chapter 1 - Introduction

1.1 Background

Since ancient times, human beings have been utilizing several methods of communication between each other. Fire was the signal form, air the transmission medium and the eyes of the observer were the receiving device. Communication systems have been improved since the late 1900's. The wire cable was used instead of air for the transmission medium owing to the invention of the telegraph in 1838, which started the new epoch of the electrical communication systems (1.1). Further, electromagnetic waves were utilized for conveying information. For larger information capacity, high frequencies (short wavelength) were employed, which led to the birth of television, radar, and microwave links. Looking at the electromagnetic spectrum (1.2), the portion of the spectrum corresponding to higher frequencies (shorter wavelengths) is the optical region from 50 nm (ultraviolet) to 100 μm (infrared). Great interest in communicating at optical frequencies was created in 1960's with the advent of the laser (1.3), which made available a coherent optical source. Later, investigation of optical fiber provided a reliable and versatile optical channel as a transmission medium by reducing the attenuation of fiber gradually. The development and

---

application of optical fiber systems grew from the combination of semiconductor technology, which provided the necessary light sources, photodetectors, and optical waveguide technology.

Since the 1970's, optical fibers have been attributed as sensors owing to their properties of environmental perturbation sensitivities. Magnetic, acoustic, pressure, temperature, displacement, acceleration, gyro, torque, current, fluid level, photo acoustic, and strain are among the fiber optic sensor types being investigated. In comparison with other sensors, optical fiber sensors offer many advantages:

- low weight and small size,
- low transmission loss and wide bandwidth,
- environmental ruggedness such as utility in high temperature, high voltage, corrosive, or other stressing environments,
- immunity to electromagnetic interference,
- geometric versatility which allows fiber sensors to be configured in arbitrary shapes.

These attractive advantages of optical fiber sensors justify the increase in the need for these sensors in such areas as aerospace, defense, manufacturing, medicine, and construction. Different types of optical fiber sensors have been developed substantially in the past few years. In the following sections, the distinct kinds of optical fiber sensors are discussed.

1.2 Classification of Optical Fiber Sensors

Optical fiber sensors can be divided into two basic classes, intrinsic and extrinsic. An intrinsic sensor relies on external perturbations directly affecting the light traveling within the optical waveguide. Mode coupling due to strain in elliptical core fibers is an example of an intrinsic effect. In extrinsic sensors, fibers are used as information carriers which transmit the optical energy altered from outside the fiber. An intensity based sensing of alignment losses between two fiber endfaces is the typical example of the extrinsic effect.

Optical fiber sensors can also be categorized into amplitude (intensity) and phase (interferometric) sensors. In the former case, the physical perturbation interacting with the fiber or some device attached to the fiber directly modulates the intensity of the light in the fiber. In the latter case, the interferometric sensor depends on some perturbation modulating the phase of the light propagating in the fiber. The advantages of intensity sensors are the simplicity of construction and implementation owing to the simple modulation techniques. Both single-mode and multimode fibers can be used. The limitation of intensity based sensors is the lesser sensitivity than the interferometric sensors. However, extreme sensitivity is not required for most applications. As these devices are competitive with existing devices, a large market appears to exist for this class of sensor.

Compared with intensity based sensors, interferometric sensors are based upon monitoring the phase of light propagating in a fiber. Thus as known, a reference light beam is required to monitor the phase of a sensing light beam. To accomplish this, phase sensors are usually constructed with two separate optical fibers, a sensing arm and a reference arm.

Light propagating through the two separate arms is combined together, and the output intensity becomes a function of the interference between the two coherent beams. When the beams are in phase, the output intensity is a maximum, and when they are out of phase, the output is a minimum. It should be mentioned that the input is single mode or linearly polarized light, as the divided sensing and reference beams have to be mutually coherent. As the phase sensor is more sensitive than the amplitude sensor, the former has been utilized extensively. The typical phase sensors are of the Mach-Zehnder and Michelson interferometric configurations. In order to explain phase sensors more clearly, the principle of interferometry with respect to the Mach-Zehnder configuration as an example is discussed in chapter 2. For the purpose of designing a new phase sensor for high temperature measurements, a new material of single crystal sapphire is introduced in chapter 3. In chapter 4, the polarimetric analysis of birefringent sapphire fiber and its application for high temperatures are discussed. The experimental setup, processing and results are also discussed. Chapter 5 forms the conclusion and discusses future developments of the research in this area of fiber optic sensors.

Chapter 2 - Principles of Interferometric Sensors

2.1 Introduction

Interferometric sensors have the highest sensitivity and best flexibility of application due to the utilization of the interference between two coherent polarized beams. Any change in the environment can be recorded as the phase difference between two arms or the interference fringes, and detected by a photodetector. The Mach-Zehnder fiber sensor is the most popular interferometric sensor, and is discussed in the following section.

2.2 Two-Arm Mach-Zehnder Fiber Interferometer

As shown in figure 2.2.1, the Mach-Zehnder fiber interferometer generally consists of two pieces of single mode fiber. The input linearly polarized light is divided into a sensing arm and a reference arm after passing through a 2 x 2 single mode fiber coupler, and combined together at the second coupler. The sensing arm experiences a perturbation environment such as temperature, pressure, strain, and electromagnetic field, which can change the length and refractive index of the fiber, and thereby the phase of the light, while the

reference arm maintains an unperturbed state. Because they carry the same single mode (treated as a plane wave), the sensing and reference arms have the same linearly polarized light leading to a stable phase difference.
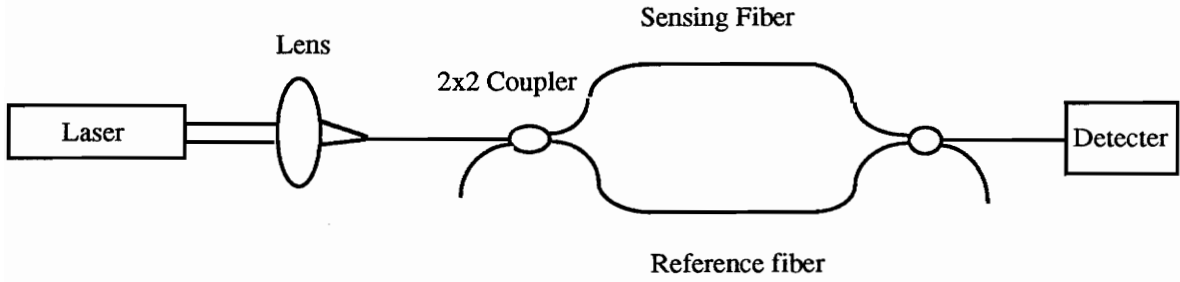
Figure 2.2.1: Two-fiber Mach-Zehnder Interferometer

A theoretical analysis (2.1) of the interferometric arrangement is presented in the following section.

The input linearly polarized light or electric field is

$$E_{in} (r, t) = E_0 \cos (k \cdot r - \omega t + \phi)$$
$$= E_0 \cos (kz - \omega t + \phi) \tag{2.2.1}$$

where E_0 is the amplitude of the light, $k = 2\pi n / \lambda$ is the propagation constant, λ is the wavelength in the vacuum, ϕ is the initial phase angle, and propagation in the z-direction along the fiber length is assumed.

The linearly polarized light in the reference arm is

$$E_r \ (\ r, t\ ) = E_{0r} \ \cos\ (\ k_r z_r - \omega t + \phi_r\ ) \tag{2.2.2}$$

The linearly polarized light in the sensing arm is

$$E_s \ (\ r, t\ ) = E_{0s} \ \cos\ (\ k_s z_s - \omega t + \phi_s\ ) \tag{2.2.3}$$

The combined amplitude at the output is

$$E_{out} \ (\ r, t\ ) = E_r \ (\ r, t\ ) + E_s \ (\ r, t\ ) \tag{2.2.4}$$

The output intensity is the time average of the output electric field squared

$$I_{out} = < E_{out}{}^2 > \tag{2.2.5}$$

where

$$\begin{aligned}
E_{out}{}^2 &= E_{out} \cdot E_{out} \\
&= E_r{}^2 + E_s{}^2 + 2\ E_r \cdot E_s
\end{aligned} \tag{2.2.6}$$

where

$$\begin{aligned}
E_r \cdot E_s &= E_{0r} \cdot E_{0s} \cos\ (\ k_r z_r - \omega t + \phi_r\ ) \cos\ (\ k_s z_s - \omega t + \phi_s\ ) \\
&= 1/2\ E_{0r} \cdot E_{0s} \ (\ \cos\ ((\ k_r z_r - \omega t + \phi_r\ ) + (\ k_s z_s - \omega t + \phi_s\ )) \\
&\quad + \cos\ ((\ k_r z_r - \omega t + \phi_r\ ) - (\ k_s z_s - \omega t + \phi_s\ ))\ ) \\
&= 1/2\ E_{0r} \cdot E_{0s} \ (\ \cos\ ((\ k_r z_r + k_s z_s\ ) + (\phi_r + \phi_s) - 2\omega t\ ) \\
&\quad + \cos\ ((k_r z_r - k_s z_s\ ) + (\phi_r - \phi_s))\ )
\end{aligned}$$

$$\tag{2.2.7}$$

After averaging Eq. (2.2.7) with respect to time we have

$$< E_r \cdot E_s > = 1/2 \, E_{0r} \cdot E_{0s} \cos ((k_r z_r - k_s z_s) + (\phi_r - \phi_s))$$

(2.2.8)

supposing that $< \cos 2\omega t > = 0$, and $< \sin 2\omega t > = 0$.

Averaging Eq. (2.2.6) with respect to time

$$
\begin{aligned}
< E_{out}^2 > &= < E_r^2 > + < E_s^2 > + 2 < E_r \cdot E_s > \\
&= < E_r^2 > + < E_s^2 > + E_{0r} \cdot E_{0s} \cos ((k_r z_r - k_s z_s) + (\phi_r - \phi_s)) \\
&= < E_r^2 > + < E_s^2 > + E_{0r} \cdot E_{0s} \cos \delta
\end{aligned}
$$

(2.2.9)

where

$$
\begin{aligned}
\delta &= (k_r z_r - k_s z_s) + (\phi_r - \phi_s) \\
&= 2\pi / \lambda \, (n_r z_r - n_s z_s) + (\phi_r - \phi_s)
\end{aligned}
$$

(2.2.10)

is the phase difference arising from initial phase angle difference $(\phi_r - \phi_s)$ and optical path length difference $(n_r z_r - n_s z_s)$ between the two arms owing to the perturbation of the sensing environment.

As mentioned in Eq. (2.2.5), I_r and I_s can be expressed as

$$I_r = < E_r^2 >$$

$$I_s = < E_s^2 >$$

and letting

$$I_{12} = 2 < \mathbf{E_r} \cdot \mathbf{E_s} > = \mathbf{E_{0r}} \cdot \mathbf{E_{0s}} \cos \delta \qquad (2.2.11)$$

Eq. (2.2.9) can be represented by

$$I_{out} = I_r + I_s + I_{12} \qquad (2.2.12)$$

Notice that if $\mathbf{E_{0r}}$ and $\mathbf{E_{0s}}$ are perpendicular, $I_{12} = 0$ and $I_{out} = I_r + I_s$, if $\mathbf{E_{0r}}$ parallels to $\mathbf{E_{0s}}$, $I_{12} = \mathbf{E_{0r}} \mathbf{E_{0s}} \cos \delta$. This can be written in a more convenient way by noticing that

$$I_r = < \mathbf{E_r}^2 > = E_{0r}^2 / 2$$

$$I_s = < \mathbf{E_s}^2 > = E_{0s}^2 / 2$$

The interference term becomes

$$I_{12} = 2 (I_r I_s)^{1/2} \cos \delta \qquad (2.2.13)$$

The output intensity is then

$$I_{out} = I_r + I_s + 2 (I_r I_s)^{1/2} \cos \delta \qquad (2.2.14)$$

When $\delta = 0$ or $2m\pi$, two arms of light are in phase, where m is an integer

$$I_{max} = I_r + I_s + 2 (I_r I_s)^{1/2} \tag{2.2.15}$$

When $\delta = 2(m+1)\pi$, two arms of light are out of phase

$$I_{min} = I_r + I_s - 2 (I_r I_s)^{1/2} \tag{2.2.16}$$

When $2m\pi < \delta < 2(m+1)\pi$, the output intensity will vary from I_{max} to I_{min}. If the amplitudes E_{0r} and E_{0s} are equal, or $I_r = I_s = I_0$, Eq. (2.2.15) can be written as

$$I = 2 I_0 (1 + \cos \delta) = 4 I_0 \cos^2 (\delta / 2) \tag{2.2.17}$$

from which it follows that $I_{max} = 4 I_0$, $I_{min} = 0$. In order to evaluate the clearness of the interference fringes, the visibility or contrast of the fringes is defined as

$$V = (I_{max} - I_{min}) / (I_{max} + I_{min}) \tag{2.2.18}$$

When the two arms of light are in phase, $I_{max} = 4 I_0$, and out of phase, $I_{min} = 0$, the interference fringes will have the maximum contrast,

$$V = 1$$

provided that the amplitudes of the signals in the two arms of light are equal; otherwise, one has

$$V < 1$$

2.3 Summary

As we discussed, the Mach-Zehnder interferometer as an example of a phase sensor, or a two-fiber interferometer has an advantage of being the most sensitive configuration for the detection of perturbations in the sensing environment. On the other hand, it has a disadvantage in that the reference arm could easily accumulate false phase information owing to the perturbation of the reference environment. Thus, extreme care must be taken to insure that no perturbation affects the reference arm of the sensor. Moreover, the two arms of the fiber interferometer require maintenance of the same state of polarization from the input over a considerably long distance. If the polarization states of the two arms are $90°$ apart, the interference term becomes

$$I_{12} = 2 < \mathbf{E_r} \cdot \mathbf{E_s} > = \mathbf{E_{0r}} \cdot \mathbf{E_{0s}} \cos \delta = 0$$

$$I_{max} = I_{min}$$

$$V = 0$$

and complete fading can result. To prevent this disadvantage, one-fiber interferometers or birefringent sensors have been invented lately. The advantage of the one-fiber interferometer is that both the interfering beams see exactly the same perturbation conditions. Another advantage is its extremely simple construction. It requires only two polarizers for the splitting and recombination of the two interfering beams. The disadvantage of the one-fiber interferometer is that it is less sensitive than the two-fiber

interferometer. The one-fiber interferometer consists of a birefringent fiber and two polarizers. It is designed on the basic principle that one fiber carries two linearly polarized beams which propagate along its slow and fast axes separately and exhibit a phase delay in response to an external force. The sapphire fiber is one of these birefringent fibers. It is a single crystal fiber possessing a large birefringence of 0.008, as well as a new material for high temperatures and high power delivery applications. Therefore, a design utilizing this sapphire fiber interferometric sensor for high temperature measurements was initiated and is discussed in chapter 4. For this purpose, the properties of birefringent single crystal sapphire fibers are introduced in the following chapter 3.

Chapter 3 - Birefringent Single Crystal Sapphire Fibers

3.1 Introduction

As optical fibers posses the attributes of low weight, small size, low power, environmental ruggedness, immunity to electromagnetic interference, good performance specifications, and low cost, optical fiber sensors have been developed rapidly in the areas of electromagnetic, acoustics, pressure, temperature, acceleration, and photoacoustic measurement. While progress has been great, the technology is not yet fully exploited. For example, silica fiber becomes soft when its operation temperature exceeds 1000 °C, so silica fiber sensors are strictly limited to low-temperature applications. As the need for optical fiber sensors in high temperatures areas such as aerospace and defense increases, a new material, sapphire fiber, has been investigated, which has a high temperature melting point of 2040° C. Sapphire fibers have not only high temperature benefits, but also many attractive chemical, mechanical, and optical properties that make them well suited for certain sensor and power delivery applications. In this chapter, this new fiber is investigated. In particular, the properties and growth methods of sapphire are discussed.

3.2 Properties of Birefringent Single Crystal Sapphire Fibers

3.2.1 Birefringent Properties of Single Crystal Sapphire

Sapphire is single crystal aluminum oxide (Al_2O_3) and exhibits anisotropic or birefringent properties. Table 3.2.1.1 lists the properties of Czochralski grown sapphire. In order to describe the birefringent properties of the single crystal of sapphire, we introduce some basic principles of this crystal.

• Uniaxial and biaxial crystal

Cubic crystals have the same dimensions in all three principal directions, and they are generally isotropic. However, most crystals are anisotropic. Those in which one dimension is different from the other two are uniaxial. Those crystals in which all three dimensions are different are biaxial. Sapphire is a uniaxial crystal because of its hexagonal crystalline structure.

• Birefringence of crystal

Birefringence or double refraction is explained by assuming that the crystal has two different indices of refraction. Thus light can be refracted into two different directions as it enters the crystal. The indices for this double refraction are referred to as the ordinary wave (o-wave) and extraordinary wave (e-wave) indices, as shown in Fig. 3.2.1.1 (b). Polarization of the o-wave is always normal to the optic z axis and its refractive index is called n_o. The polarization of the e-wave is generally at an angle to z, and its
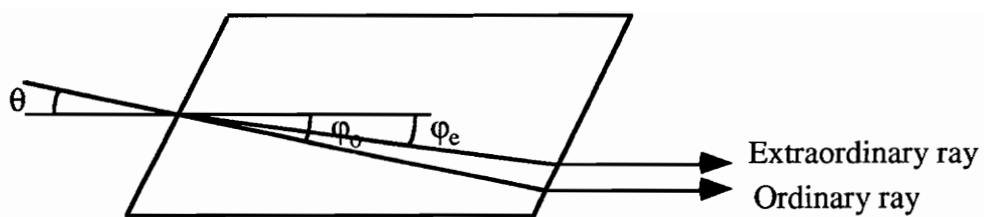
Figure 3.2.1.1(a): Double refraction in a calcite prism
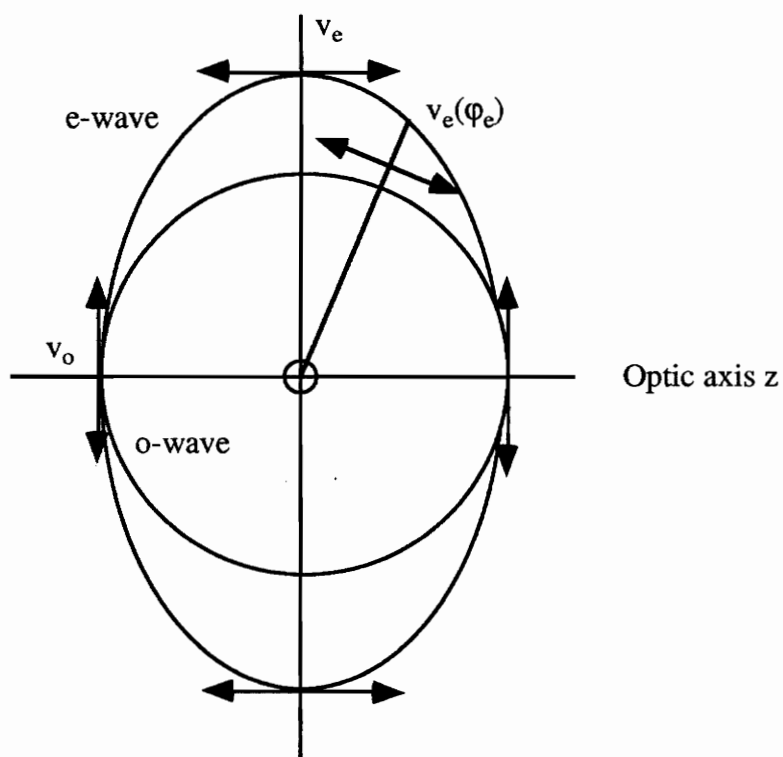
Figure 3.2.1.1(b): Wavelets in a negative uniaxial crystal

refractive index is called $n_e(\varphi_e)$, when its polarization is parallel to z, its refractive index is called n_e. Using Snell's law, we have

$$\sin \theta / \sin \varphi_o = n_o \qquad (3.2.1.1)$$

and

$$\sin \theta / \sin \varphi_e = n_e(\varphi_e) \qquad (3.2.1.2)$$

The extraordinary index $n_e(\varphi_e)$ depends on the direction of propagation φ_e, as shown in Fig. 3.2.1.1.(a). If $n_e > n_o$ the crystal is called positive; otherwise, it is termed negative.

• The optic axis

There is one (two) direction of propagation in a uniaxial (biaxial) crystal for which double refraction does not occur. This is the direction of the optic z axis, and the index of refraction for both polarizations is n_o for propagation along this axis.

• The index ellipsoid

The index of refraction for different polarizations can be represented by the distance from the center of an ellipsoid to this surface , as is seen in Fig. 3.2.1.2. For propagation down one axis, say x, there is a value of n for the y component (polarization in the y direction) of electric field, E_y, and another for E_z. These will be plotted on the y and z axes, respectively. Since the index depends on the polarization of the wave but not on its direction of propagation, the axes of the ellipsoid refer to polarization states.

For cubic crystals, $n_x = n_y = n_z$, and the index ellipsoid degenerates into a sphere, but in a uniaxial crystal, $n_x = n_y$, so that the figure representing these materials is an ellipsoid of revolution. For biaxial crystals, each value of n is different and we have a general ellipsoid.

Cubic   Uniaxial   Biaxial
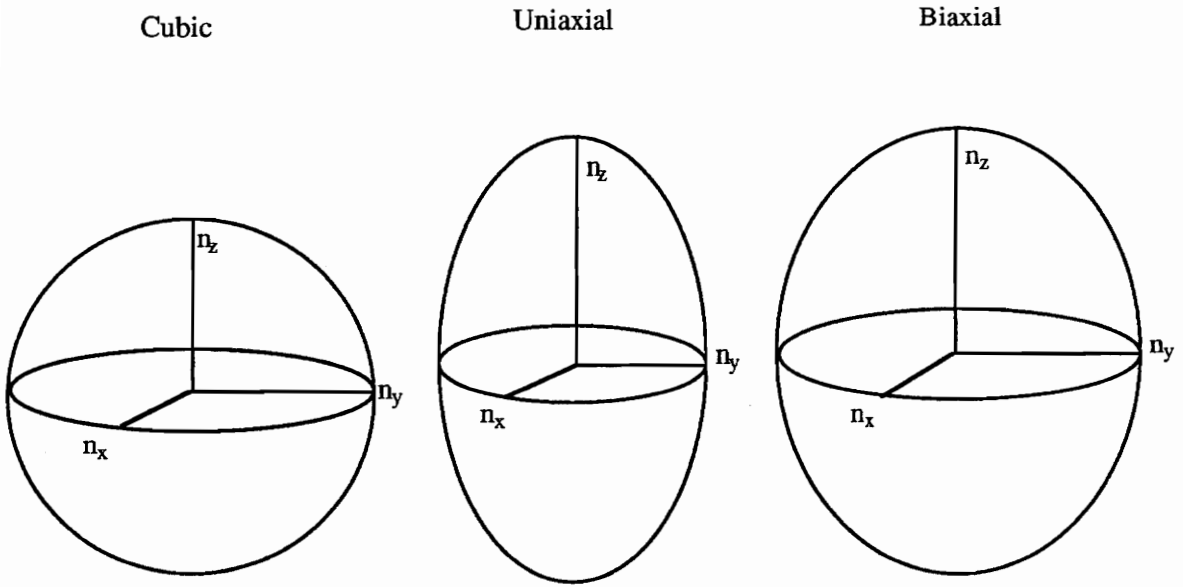
Figure 3.2.1.2: The index ellipsoid for different symmetries

In uniaxial crystals, for propagation in the z-direction (the optic axis), the indices of refraction are represented by the x, y plane. The figure circumscribed is a circle, indicating that both polarizations have the same value of n_o. For propagation along x, on the other hand, the intersection with the surface is an ellipse, giving distinct values for n_o and n_e. As the direction of propagation changes in the xz plane, one index is always n_o but the other changes from n_e to n_o. Thus, the extraordinary index depends on the direction of propagation and is given by the equation

$$1 / (n_e^2 (\theta)) = (\cos^2 \theta) / n_o^2 + (\sin^2 \theta) / n_e^2 \qquad (3.2.1.3)$$

where θ is the angle between the optic axis and $\mathbf{k}$ (the vector propagation constant). This is summarized in Fig. 3.2.1.3, where the two values of n are plotted for each direction of propagation. At $\theta = 0$, both indices are shown equal to n_o.
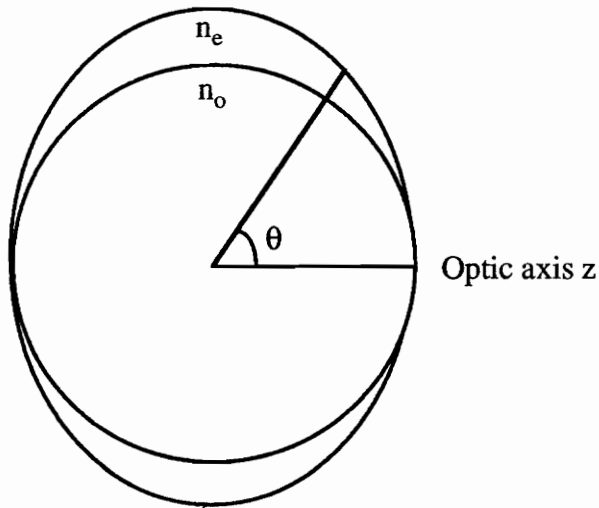
Figure 3.2.1.3: Plot of two indices of refraction for a wave propagating in a uniaxial crystal. θ is the direction of propagation with respect to the optic z axis.

• Birefringence of a single crystal of sapphire

Sapphire is a negative single crystal for $n_e < n_o$ (n_e=1.760, n_o=1.768), with a difference between refractive indices of 0.008. The axis along which the polarization has the refraction index n_o is called the slow axis. On the other hand, the axis along which the polarization has the refraction index n_e is called fast axis. The yz plane of the index ellipsoid of a negative single crystal sapphire is shown in Fig. 3.2.1.4. It is noted that the polarization properties of the sapphire crystal depend on the shape of the index ellipsoid. If the refractive index of the crystal is not changed with the application of an external effect, the shape of the index ellipsoid will be stable. When linearly polarized light is propagated along either the slow (n_o) or fast (n_e) axis of the crystal, linear polarization will be maintained during an external effect.
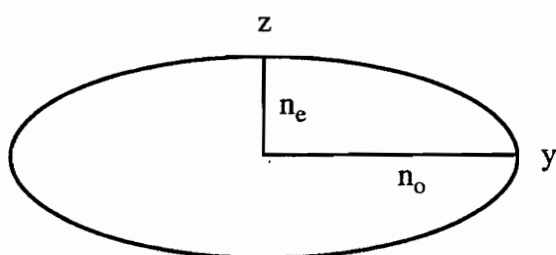
Figure 3.2.1.4: The yz plane of the index ellipsoid of

the negative single crystal sapphire

3.2.2 Chemical Properties of Sapphire Fibers

Sapphire is chemically resistant, insoluble, bio-inert and nontoxic. Because of these properties sapphire fiber can be used in corrosive environments and medical applications. This is in direct contrast to moisture-sensitive, heavy metal fluoride glass fibers, like ZBLAN (which is a fluorozirconate glass), sapphire fibers can be used in direct contact with tissue.

3.2.3 Mechanical Properties of Sapphire Fibers

Sapphire fibers are mechanically strong and can be bent to a radius of less than 10 mm without breaking (3.1). Originally, sapphire fibers were manufactured for the reinforcement of metal-matrix composites. They are also very stiff, having a Young's modulus nine times larger than that of glass (3.2). As the fibers are nontoxic and very strong, they seem ideal for use in medical delivery systems.

3.2.4 Optical Properties of Sapphire Fibers

Sapphire has a wide transparency region in the spectrum, ranging from 0.3 μm to 4 μm. Thus sapphire fibers are an excellent choice for the transmission of Er: YAG laser energy at 2.94 μm for surgical applications. Sapphire's optical properties include its attenuation versus wavelength, which depends on scattering losses and absorption losses.

• Scattering losses are affected by the uniformity and cleanliness of these unclad fibers. The easiest way to decrease these losses is by heating the sapphire fiber using a torch, and cleaning these fibers with methanol before use. Further needed improvement through decreasing the scattering losses can be made by cladding the fibers. Scattering loss was measured at different wavelengths ranging from blue to the near infrared. The results are shown in table 3.2.4.1.

• Absorption losses are also affected by the cleanliness and surface quality of the fiber. These losses can be measured with high sensitivity using laser calorimetry (3.3). The results of absorption measurements at six different wavelengths are shown in table 3.2.4.1 and figure 3.2.4.1.
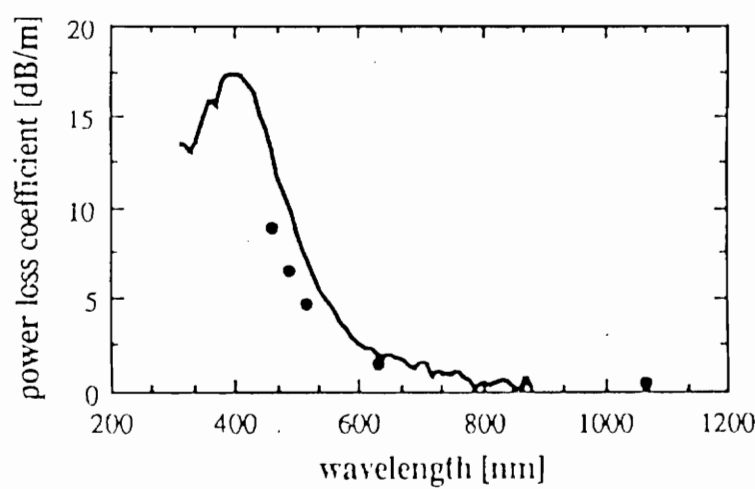
Fig. 3.2.4.1: Absorption measurements at six different wavelengths

Table 3.2.4.1 indicates that absorption dominates scattering losses strongly in the mid-infrared. In the near-infrared, absorption is small and comparable in magnitude to the scattering losses.

From figure 3.2.4.1, there is a broad absorption band centered at 400 nm, with a peak absorption of 0.04 cm^{-1}. It would limit the use of the sapphire fibers for work in the UV and the blue-green region. This band has been reported in γ irradiated crystal and can be explained by the presence of OH$^-$ centers (3.4). An improvement has been made when the fiber was grown in an atmosphere of pure oxygen, with absorption loss at the Er: YAG line of 0.88 db/m (3.5). It is conjectured that annealing in a reactive atmosphere to control the OH$^-$ concentration might remove the color centers and reduce the absorption considerably (3.6). Another phenomenon should be noted that the absorption coefficient of sapphire is increased for increasing temperature, as shown in Fig. 3.2.4.2 and table 3.2.4.2. The transmission of sapphire is shown in Fig. 3.2.4.3.
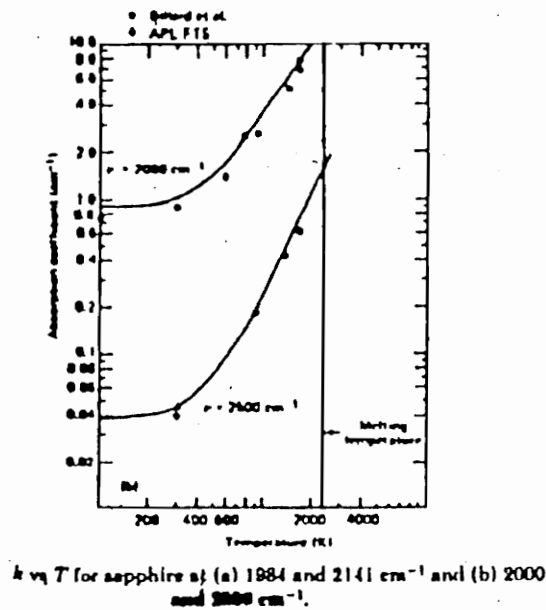
Fig. 3.2.4.2: Absorption coefficient vs. temperature
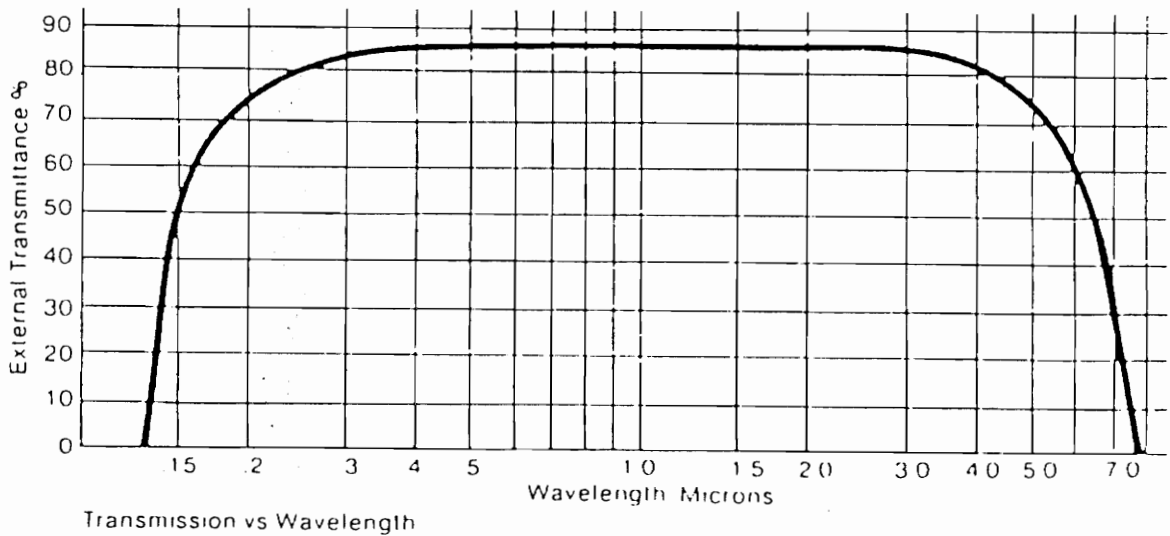
Fig. 3.2.4.3: Transmittance for Sapphire

3.2.5 *Physical Properties of Sapphire Fibers*

The physical property of a high temperature melting point of 2040 °C enables sapphire fibers to be used in high temperature (>1000 °C) applications. In high temperature measurements the index difference or birefringence ($\Delta n = n_o - n_e$) as a function of temperature is very important. Experimental results indicate that n_o and n_e increase when the temperature is increased, as is shown in Fig. 3.2.5.1. Results also suggest that the birefringence increases when the temperature is increased but the change of the birefringence dependence on temperature is small.

Δn (10⁻²) ... $\Delta n\ (10^{-2})$

2

1

0   200   400   600   800   T (°C)

80

o a
+ b

60

$\Delta n\ (10^{-3})$

40

20

0   100   200   300   T (°C)
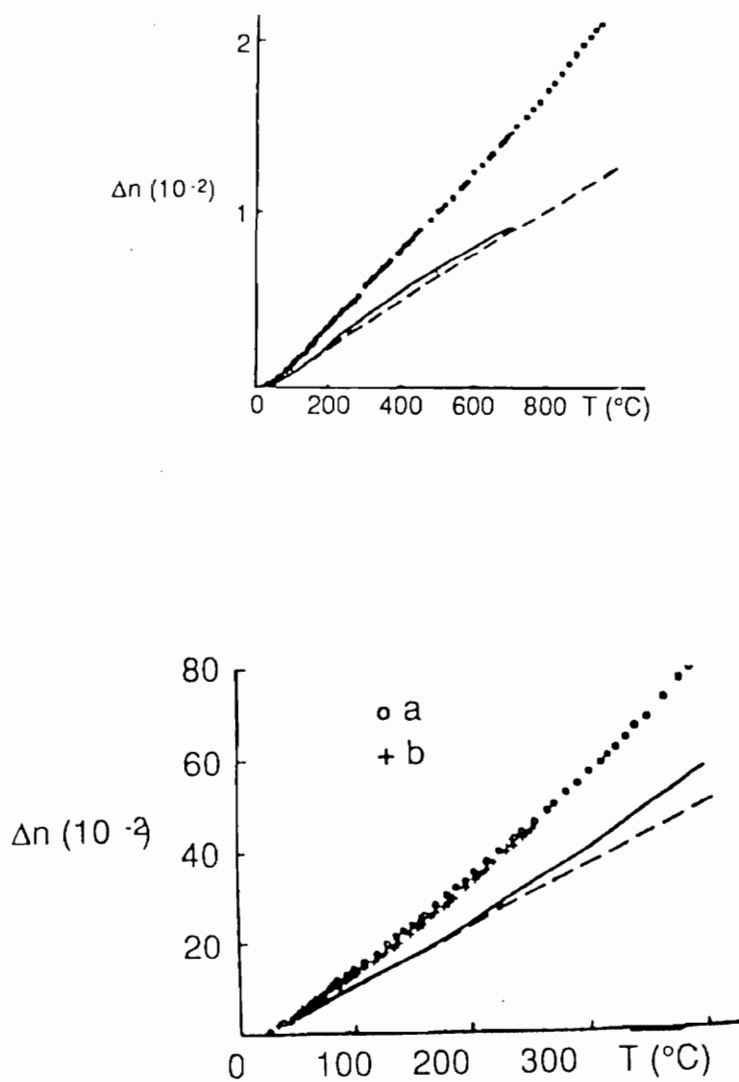
Fig. 3.2.5.1: Temperature dependence of refractive indices n_o (a) and n_e (b)

for $\lambda = 579.1$ nm

This property indicates that the shape of the index ellipsoid of crystal sapphire fiber has a small change in high temperatures. Thus, when linearly polarized light propagates along one of the principal axes of the sapphire fiber the state of the linear polarization will be partially maintained at high temperatures.

3.2.6 Properties of Teflon-clad Sapphire Fibers

Sapphire fibers are normally grown as core-only fibers, which have large losses. Cladding is effective in preventing leakage of energy from these fibers into absorbing environments that may surround the fiber. The Teflon-clad sapphire fiber, Teflon-FEP (perfluorinated ethylene propylene) when applied to sapphire fiber as a cladding, has the following properties:

• the infrared spectrum of Teflon-FEP shows that the strong absorption bands of FEP lie in the spectral region beyond the 3.5 μm wavelength shown in Fig. 3.2.6.1. The strong absorption at 3.5 μm is due to C-F bonds' absorption,

• teflon cladding can protect sapphire fibers from environmental absorption and perturbation, and

• bending losses are due to the energy coupling into the Teflon cladding.
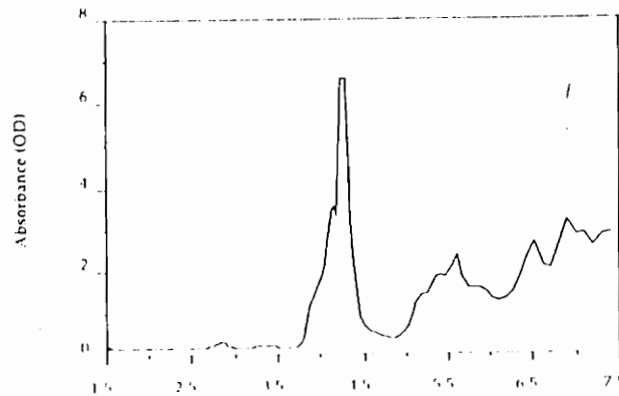
Fig. 3.2.6.1: Infrared absorption spectrum of Teflon-FEP

3.3 Growth Methods of Sapphire Fibers

3.3.1 Growth Methods of Core-only Sapphire Fibers

The growth of core-only sapphire fibers can be divided into two primary methods (3.7):

• The pulling of fibers either from molten starting materials or from the molten zone of crystal ingots,

• The recrystallization of polycrystalline fibers.

Growth methods can also be categorized according to type of growth technique; there are four main groups (3.8):

• Bridgman melt method,

• Czochralski melt method,

• floating zone methods, and

• Verneulli vapor process.

In growing single crystal from a melt, one end of a seed crystal is placed at or near a molten material. The other end of the seed crystal is placed in direct contact with a heat sink, allowing extraction of heat through the growing crystal. Heat must be removed, while at the same time preventing supercooling which causes competing crystals to nucleate. The seed crystal also determines crystal axis orientation.

The Verneulli vapor process method is to control the condensation of vapors. In the Verneulli flame fusion process, a flame gives off combustion products with the desired composition. These combustion products then condense on a seed crystal, initiating an epitaxial growth.

There are also two other methods:

• The laser heated pedestal growth (LHPG) method (3.9), and

• Stepanov's method (3.10).

In the LHPG method, the tip of a rod of source material is heated by a focused CO_2 laser, forming a molten liquid droplet. By dipping an oriented seed crystal (whose c-axis is along the growth axis) into the droplet, a suspended molten zone is produced with a shape governed by surface tension. Growth can then be started, by carefully controlling the ratio of the speeds at which a source rod is pushed into the zone and the fiber is pulled out, as

shown in Fig. 3.3.1.1. The fibers grown should be of the same purity as the source-material since there is no contact of the liquid zone with crucibles or dies. Another new LHPG technique is introduced in reference (3.11).

In Stepanov's method, capillaries and dies are used to control the growth of single crystal fibers. More information can be found in standard books on crystal growth (3.12-3.13).
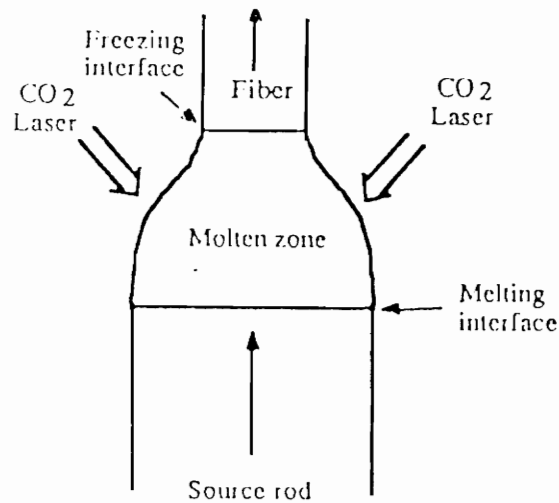
Fig.3.3.1.1: The laser-heated pedestal growth process

3.3.2 Growth Method of Teflon-clad Sapphire Fibers

The growth of Teflon-clad sapphire fibers is a new technique. Many concepts, such as ion

diffusion (3.14) and polymer cladding, have been mentioned for preparing core-clad sapphire structures. The molten zone, from which the crystal fibers are pulled, contains rapidly moving convective flow patterns that prohibit the growth of core-clad fibers from rod-in-tube source rods. Once the source rods were melted, their geometry was lost, and the composition of the fiber that grows was essentially that of the entire molten zone. The method explored for cladding sapphire fibers was melt extruding perfluorinated ethylene propylene (Teflon-FEP 100) onto the core-only fiber. A small piston drive extruder was fitted with a commercial crosshead to hot extrude Teflon onto the fiber. The extrusion temperature was 385 °C, and the coating speed was about 1 m / min.

3.4 Conclusion

Several properties of sapphire fibers enable them to be applicable in high-temperature and rugged environments: its melting point of 2040 °C and the chemical resistance. Several methods of growing single crystal sapphire fibers were also introduced. Comparatively, the cost of sapphire fibers is more than that of silica fibers, but the special applications of sapphire fibers more than compensates for the additional cost. The fact that the small change in birefringence at high temperatures suggests that states of linear polarization will be partially maintained in high temperatures. In order to utilize these properties for special applications, polarimetric analysis and optical sensors for high temperatures are explored and discussed in the following chapter.

Table 3.2.1.1: Properties of Czochralski Grown Sapphire

Properties of Cz Sapphire

Physical

Density	3.99 g/cm^3
Hardness	Mohs 9 (by definition)
	Knoop microindenter:
	1600 - 2200
Melting point	2040°C
Compressive strength	400,000 psi
Young's modulus	(50 - 56) × 10^6 psi
Tensile strength	
at 20°C	58,000 psi (design minimum)
at 500°C	10,000 psi (design minimum)
at 1000°C	52,000 psi (design minimum)
Modulus of rupture	65 - 100,000 psi
(maximum bending stress	
is orientation dependent)	
Modulus of rigidity	27 × 10^6 psi

Thermal

Conductivity	
(60° orientation)	
at 0°C	0.11 cal/cm°C sec
at 100°C	0.06 cal/cm°C sec
at 400°C	0.03 cal/cm°C sec
Specific heat	
at 20°C	0.10 cal/g
Heat capacity	
at 20°C	78 abs J/deg mol
at 1000°C	125 abs J/deg mol
Average coefficients of	
thermal expansion	
(60° orientation)	
20 - 50°C	5.8 × 10^{-6} cm/cm °C
20 - 500°C	7.7 × 10^{-5} cm/cm °C

Electrical

Volume resistivity	
at 25°C	10^{14} Ω/cm

Dielectric constant and dielectric loss tangent at 25°C		$\varepsilon \perp C$	$\varepsilon \parallel C$
K	1 MHz	9.39	11.58
	3 GHz	9.39	11.58
8.5 GHz	9.39	11.58
tan δ	1 MHz	0.0001	< 0.0001
	3 GHz	< 0.0001	< 0.0001
8.5 GHz	< 0.00002	< 0.00005
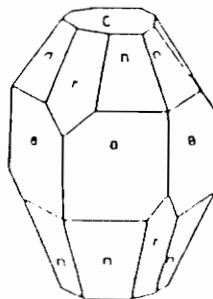
Sapphire, single crystal aluminum oxide, is classed as a rhombohedral structure but is normally indexed on hexagonal axes. Optically, it is a negative, uniaxial crystal in the visible; it exhibits anisotropy in its physical, thermal, and dielectric properties. An amphoteric semiconductor, sapphire's energy band gap, approximately 10 eV, which is one of the largest for oxide crystals, permits useful optical transmission to extend from about 1450 Å to 5.5 μm.

Table 3.2.4.1: Results of the loss measurements made for fibers grown in air.

The data in parenthesis was measured for a fiber grown in oxygen.

Wavelength nm	Scattering loss dB/m	Wavelength nm	Absorption loss dB/m
457.9	0.156±0.02	457.9	17.4 ±0.8
488.0	0.174±0.02	488.0	6.30±0.09
514.5	0.156±0.02	514.5	4.6 ±0.15
632.8	0.130±0.02	632.8	1.3 ±0.2
1064	0.178±0.03	1064	0.28±0.08
		2936	1.7 ±0.2 (0.88±0.2)

Table 3.2.4.2: Experimental Sapphire Absorption Coefficient

ν (cm^{-1})	k (cm^{-1})		
	$T = 295$ K	$T = 582$ K	$T = 775$ K
1699	3.61	7.38	11.6
1796	2.75	4.37	7.59
1892	1.66	2.53	4.52
1988	0.99	1.50	2.81
2085	0.60	0.91	1.74
2181	0.34	0.52	1.08
2278	0.18	0.29	0.63

Chapter 4 - Experimental Setups, Results and Analyses

4.1 Introduction

As we mentioned in chapter 2, one-fiber Mach-Zehnder interferometers or birefringent fiber sensors offer the advantage of both arms having exactly the same perturbation conditions as well as simple construction. The construction requires only one fiber and two polarizers for the splitting and combination of the two coherent signals from the linearly polarized input. Sapphire fiber is one of the birefringent fibers which can constitute this sensor. In this sensor, two orthogonally polarized signals propagate along the slow and fast axes of the birefringent fiber separately and produce a phase delay dependent upon the refractive index and path difference, which in turn are affected by the external perturbation. They are combined into different elliptical signals before the analyzer and interference after the analyzer. This kind of sensor can also be called a birefringent fiber polarimetric interferometer because the variation of output polarization states is exploited as a measure of the magnitude of an external effect. As sapphire is well-known for high temperatures, a birefringent sapphire fiber polarimetric interferometer for high temperatures is designed and discussed in this chapter.

4.2 Polarization of Light

The states of polarization are basic properties of the light, and they are often used in the polarimetric interferometer. Before discussing this sensor the introduction of the polarization properties of light is required.

Polarization is one of the most important properties of light. The states of polarization are linear, elliptical, or circular.

4.2.1 Linear Polarization

A plane or linearly polarized electric wave traveling in the z direction can be represented by

$$E\ (r, t) = E_0 \cos(\omega t - k \cdot r + \phi)$$
$$= E_0 \cos(\omega t - kz + \phi) \qquad (4.2.1.1)$$

The components of the electric field can be expressed as

$$E_x\ (z, t) = E_{0x} \cos(\omega t - kz) \qquad (4.2.1.2)$$

and

$$E_y\ (z, t) = E_{0y} \cos(\omega t - kz + \delta) \qquad (4.2.1.3)$$

where E_x and E_y represent the electric fields in the x and y directions separately, E_{0x} and E_{0y} are the corresponding amplitudes, $\omega = 2\pi f$, where f is the frequency of the light, $k = 2\pi / \lambda$, which is the wave propagation constant with λ being the wavelength of the light, δ is the relative phase difference between the waves, providing that one of the initial phase angle of the electric field component is zero. The resultant wave of the two orthogonally independent components is then simply

$$E(z,t) = E_x(z,t) + E_y(z,t) \qquad (4.2.1.4)$$

If δ is zero or an integer multiple of 2π, the two components are in phase. Equation (4.2.1.4) is then also a linearly polarized wave with a polarization vector making an angle

$$\theta = \arctan(E_{0y} / E_{0x}) \qquad (4.2.1.5)$$

with respect to the x axis, and having a magnitude

$$E = (E^2_{0x} + E^2_{0y})^{1/2} \qquad (4.2.1.6)$$

This case is shown schematically in Fig. 4.2.1.1. Conversely, just as any two orthogonal plane waves can be combined into a linearly polarized wave, an arbitrary linearly polarized wave can be resolved into two independent orthogonal plane waves that are in phase.
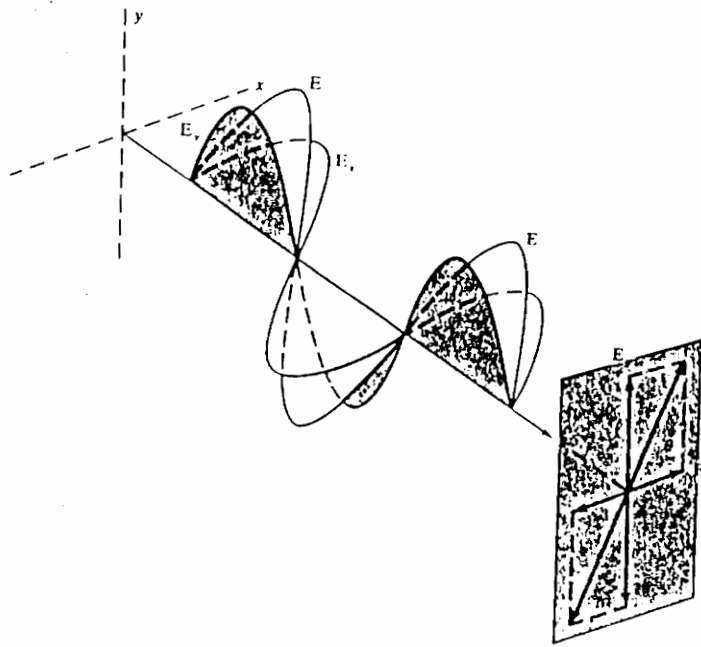
Fig.4.2.1.1: Addition of two linearly polarized waves

having zero relative phase between them

4.2.2 Elliptical and Circular polarizations

For general values of δ and θ the wave given by Eq. (4.2.1.4) is elliptically polarized. The resultant field vector **E** will both rotate and change its magnitude as a function of the angular frequency ω. From Eqs. (4.2.1.2) and (4.2.1.3) we can show that for any general value of δ

$$(E_x / E_{0x})^2 + (E_y / E_{0y})^2 - 2 (E_x / E_{0x}) (E_y / E_{0y}) \cos \delta = \sin^2 \delta$$

$$(4.2.2.1)$$

which is the general equation of an ellipse. Thus as Fig. 4.2.2.1 shows, the endpoint of **E**

---

will trace out an ellipse at a given point in space. The axis of the ellipse makes an angle α relative to the x axis given by

$$\tan 2\,\alpha = (\,2\,E_{0x}\,E_{0y}\cos\delta\,)\,/\,(\,E^2_{0x} - E^2_{0y}\,) \qquad (4.2.2.2)$$

To get a better picture of Eq. (4.2.2.1), let us align the principal axis of the ellipse with the x axis. Then $\alpha = 0$, or equivalently, $\delta = (2m+1)\,\pi\,/\,2$, where m is integer, so that Eq. (4.2.2.1) becomes

$$(\,E_x\,/\,E_{0x}\,)^2 + (\,E_y\,/\,E_{0y}\,)^2 = 1 \qquad (4.2.2.3)$$

This is the equation of an ellipse with the origin at the center and semiaxes E_{0x} and E_{0y} . When $\theta = 45°$, $E_{0x} = E_{0y} = E_0$

$$E_x{}^2 + E_y{}^2 = E_0{}^2 \qquad (4.2.10)$$

circularly polarized light is formed.
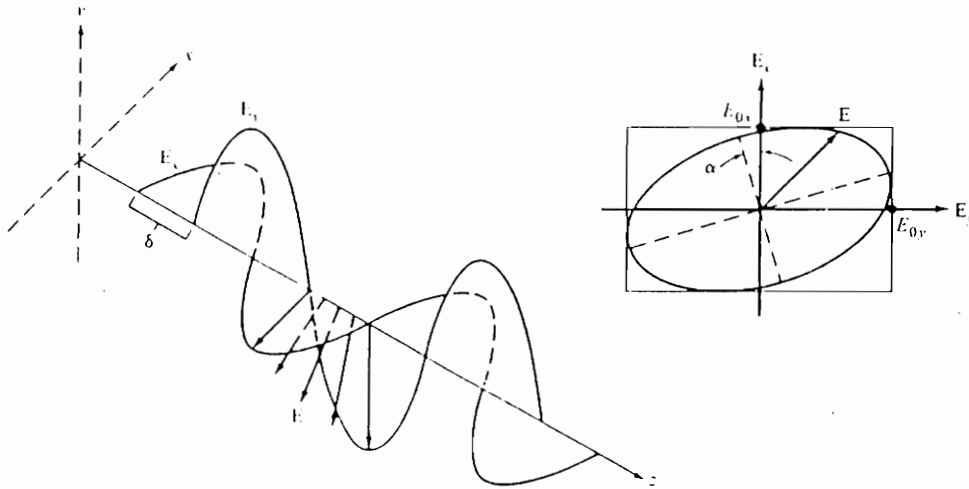
Fig. 4.2.2.1: Elliptically polarized light results from the addition of two linearly polarized waves of unequal amplitude having a nonzero phase difference δ between them

4.3 The Birefringent Sapphire Fiber Polarimetric Interferometer

The birefringent sapphire fiber polarimetric interferometer is the same as the one-fiber Mach-Zehnder interferometer. It consists of two polarizers and one piece of sapphire fiber which is positioned between the former, as shown in Fig. 4.3.1. A linearly polarized light of amplitude E_0 with an angle θ to the fiber principal axis (slow axis) is split into two orthogonally polarized components propagating along the slow axis of x and fast axis of y separately. The amplitudes of the components are $E_0 \sin \theta$ and $E_0 \cos \theta$. A phase delay δ is produced at the end of the fiber because of the difference of refractive indices between the two components and the length of the fiber, which is expressed as

$$\delta = 2\pi \, (n_0 - n_e) \, L / \lambda = 2\pi \, \Delta n \, L / \lambda \tag{4.3.1}$$

The two orthogonally polarized components are combined into different polarized signals before passing the analyzer, which are dependent on the phase difference δ. If $\delta = m\pi$, where m is zero or integer, the light is linear; if $\delta = (2m+1)\pi/2$, it is circular for $\theta = 45°$, otherwise, it is elliptical light. The two orthogonally polarized signals are decomposed after passing the analyzer, and then interfere owing to their coherence. Φ is the angle between the slow axis x of the fiber and the transmission axis p_2 of the analyzer. The plot of decomposition is shown in Fig. 4.3.2. The amplitudes of the decomposed components are $E_0 \sin\theta \sin\phi$ and $E_0 \cos\theta \cos\phi$.

According to the Eq. (2.2.14), the output intensity of the polarimetric interference is represented by

$$
\begin{aligned}
I_{out} &= (E_0 \sin\theta \, \sin\phi)^2 + (E_0 \cos\theta \, \cos\phi)^2 - 2 \, E_0^2 \, (\sin\theta \, \sin\phi \, \cos\theta \, \cos\phi) \cos \delta \\
&= I_0 \, (\cos^2 (\theta + \phi) + \sin 2\theta \, \sin 2\phi \, \sin^2 (\delta/2))
\end{aligned}
$$

$$\tag{4.3.2}$$
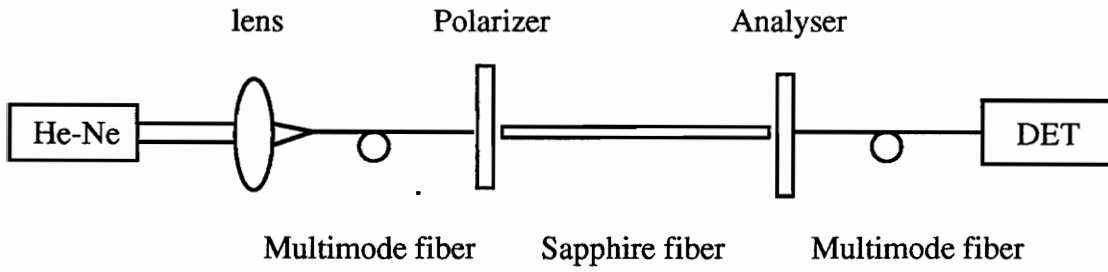
where I_0 is the input intensity.

Fig.4.3.1: Geometry of the birefringent fiber polarimetric interferometer
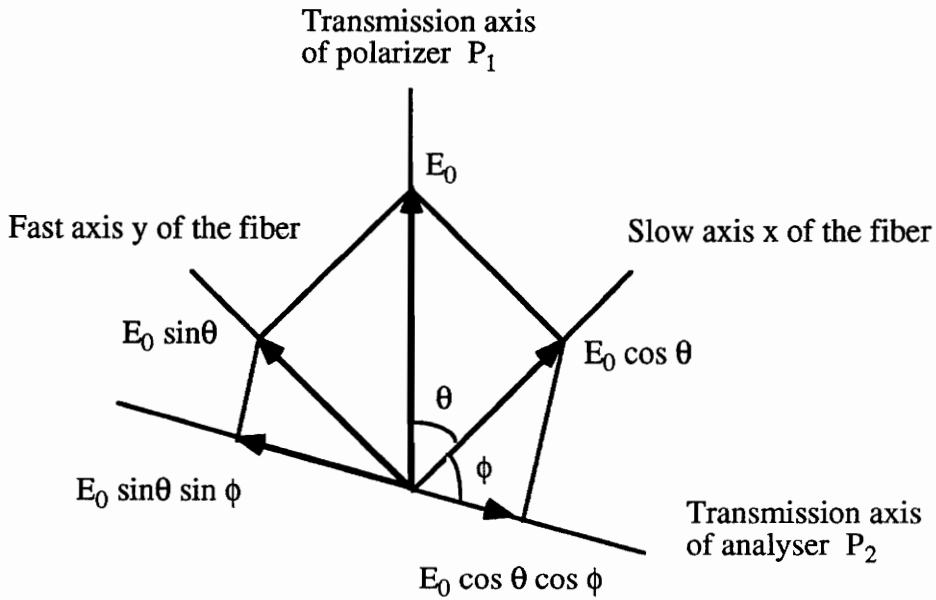and setup of sapphire fiber sensor for polarimetric analyses

Fig. 4.3.2: Geometry of decomposition of input linearly polarized light
for the birefringent fiber polarimetric interferometer

4.4 Polarimetric Analyses of Single Crystal Sapphire Fibers

4.4.1 Introduction

Since the sapphire fiber is a natural birefringent single crystal, as we mentioned in chapter 3, it can be used as a birefringent fiber polarimetric phase interferometer, in which the output polarization state can be changed due to an external effect. Many papers have exploited the polarimetric properties and applications of single-mode birefringent induced fibers in recent years (4.1-4.10), but the sapphire fiber has not yet been investigated. Sapphire fibers are bare multimode fibers about 100 μm in core diameter. In order to employ multimode sapphire fibers for high temperatures using the polarimetric interferometric method, an investigation of the polarimetric properties of sapphire fibers is required. The experiment conducted and analyses produced are described in the following subsections.

4.4.2 Setup

As shown in Fig. 4.3.1, a He-Ne laser with a 5 mw output at $\lambda = 0.6328$ μm was used as a light source. A piece of sapphire fiber was sandwiched between two polarizers. After coupling into a 100/140 μm multimode fiber connected to the polarizer, the light passed through the polarizer, and was then coupled into the sapphire fiber. The exiting light from the fiber passed through the analyzer and was coupled into another multimode fiber

terminating at the photodetector.

4.4.3 Processing and Results

As was discussed in section 4.3, for arbitrary δ and θ, the two orthogonally polarized components are combined into generally elliptical light before passing the analyzer. When the linearly polarized light is launched in such a way that the polarization is parallel to the slow or fast axis (principal axis) of the sapphire fiber, a state of linear polarization is obtained. However, when the polarization is launched at an angle θ to the principal axis, the polarization state will change periodically from linear to elliptical to linear. After passing through the analyzer the output interference intensity follow Eq. (4.3.2) and is expressed as

$$I_{out} = I_0 \left(\cos^2 (\theta + \phi) + \sin 2\theta \sin 2\phi \sin^2 (\delta/2) \right)$$
$$= I_0 \left(\cos^2 (\theta + \phi) + \sin 2\theta \sin 2\phi \sin^2 (\pi \, \Delta n \, L / \lambda) \right)$$

$$(4.4.3.1)$$

where I_0 is the intensity of input linearly polarized light, $\delta = 2\pi \, \Delta n \, L / \lambda$ is the phase difference, θ (or ϕ) is the angle between the transmission axis P_1 (or P_2) of the polarizer (or analyzer) and the slow axis of the fiber, L is the propagation length of the light in the fiber, λ is the operating wavelength in vacuum, and Δn is the birefringence of the sapphire fiber. It is clear that the output intensity follows a squared sinusoidal variation which depends on the angle θ and ϕ, and the phase difference δ. Since the

relative optical path ΔnL is a function of the measurand properties that in turn are due to factors such as the Kerr and Pockels effects, photoelasticity, strain, pressure or temperature, the output intensity is a sine squared function of the measurand if the angles θ and ϕ are not changed. In a high temperature experiment, ΔnL is dependent on the temperature, and the output intensity is a squared sinusoidal function of temperature when the angles θ and ϕ are fixed. However, at room temperatures without other external effects, ΔnL is constant, and the output intensity is just a squared sinusoidal function of θ and ϕ. When the angle $\phi = 0°$ or $90°$, the transmission axis of the analyzer P_2 is rotated parallel or perpendicular to the slow axis of the fiber (there is no decomposition on the P_2), and the state of output polarization is generally an ellipse dependent on the angle θ, as shown in Fig. 4.4.3.1. The output intensity is then reduced to Marlus' law

$$I_{out} = I_0 \cos^2 \theta \qquad\qquad (4.4.3.2)$$

where $\phi = 0°$, and

$$I_{out} = I_0 \sin^2 \theta \qquad\qquad (4.4.3.3.)$$

where $\phi = 90°$

In our experiment, when θ was rotated to $0°$, $90°$, $180°$, or $270°$, that was, when the linear polarized light propagated along the slow or fast axis of the fiber, the output polarization was linear; otherwise, elliptical. Output intensity varied sinusoidally as θ changed from $0°$ to $360°$, as is shown in Fig.4.4.3.2 (a) (1). The good, but not ideal periodic sinusoidal variation indicates that the linear polarization was maintained partially. The degree

of linear polarization is defined as

$$P = (I_{max} - I_{min}) / (I_{max} + I_{min})$$ (4.4.3.4)

where I_{max} and I_{min} are the maximum and the minimum output intensity, respectively.

To get a good curve of sinusoidal variation, the launching condition must be accurate, otherwise, the curve would not follow the sinusoidal variation shown in Fig.4.4.3.2 (b) (1). The corresponding intensity distribution of the good curve under the accurate launching condition was essentially a uniform pattern with stronger intensity in the center than the surrounding area, as is shown in Fig.4.4.3.2 (a) (2), and the the poor curve under the offset launching condition was a donut-like pattern shown in Fig.4.4.3.2 (b) (2). It was also observed that the quality of the curve and field distribution were dependent on not only the launching condition but also on the core diameter, length, and surface uniformity of the sapphire fiber. Figure 4.4.3.2 shows the results of a tested fiber 7 cm in length, 97 μm in diameter, 0.5 dB/m in attenuation, produced by the manufacturer USF. Comparatively, Fig.4.4.3.3 corresponded to a sapphire fiber which was 32 cm in length, 112 μm in diameter, 3.7 dB/m in attenuation, and produced by the same manufacturer, USF. According to Eq. (4.4.3.4) the polarization extinction ratio tested is 6 dB for the fiber 7 cm long, and is 3 dB for the fiber 32 cm long.
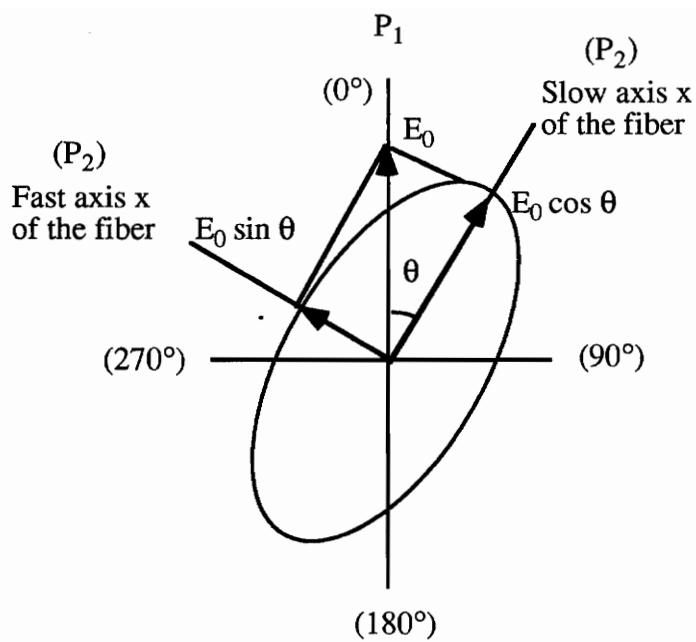
Fig. 4.4.3.1: The states of output polarization after linearly polarized light passes through the sapphire fiber polarimetric interferometer ($\phi = 0°$ or $90°$) (The principal axis of the ellipse is aligned with the x axis)

Figure 4.4.3.2 (a) (1)

Fig.4.4.3.2.(a) (1): The curve showing sinusoidal variation of output

intensity under the onset launching condition

(sapphire fiber 7 cm in length)

Fig. 4.4.3.2 (a) (2): The field distribution showing sinusoidal variation of

output intensity under the onset launching condition

(sapphire fiber 7 cm in length)

Figure 4.4.3.2 (b) (1)

Fig. 4.4.3.2 (b) (1): The curve showing sinusoidal variation of output

intensity under the offset launching condition

(sapphire fiber 7 cm in length)

Fig. 4.4.3.2 (b) (2): The field distribution showing sinusoidal variation of

output intensity under the offset launching condition

(sapphire fiber 7 cm in length)
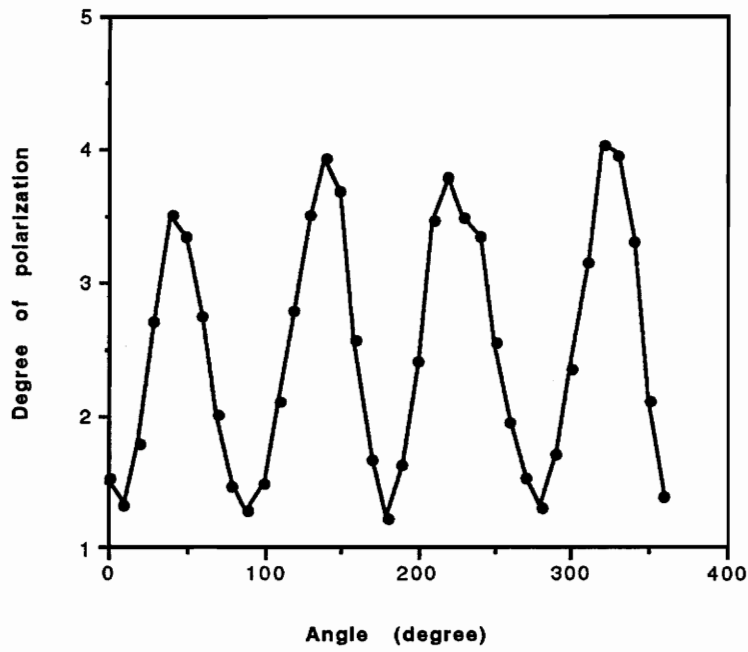
Figure 4.4.3.3 (a) (1)

Fig.4.4.3.3.(a) (1): The curve showing sinusoidal variation of output
intensity under the onset launching condition
(sapphire fiber 32 cm in length)

Fig. 4.4.3.3 (a) (2): The field distribution showing sinusoidal variation of
output intensity under the onset launching condition
(sapphire fiber 32 cm in length)

Figure 4.4.3.3 (b) (1)

Fig. 4.4.3.3 (b) (1): The curve showing sinusoidal variation of output

intensity under the offset launching condition
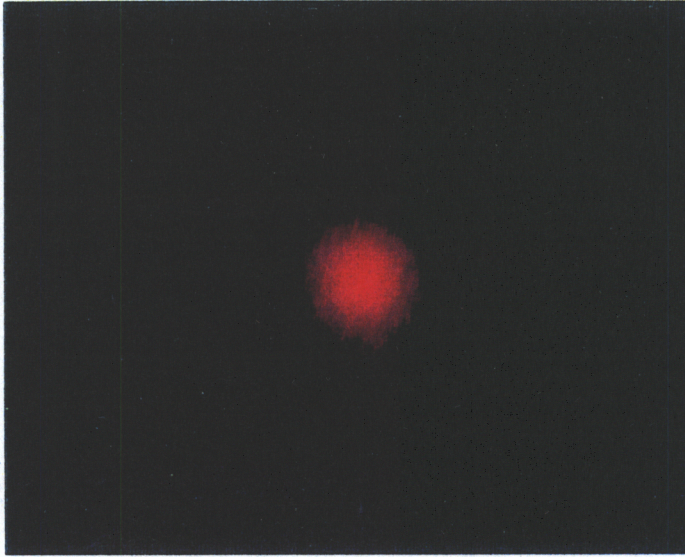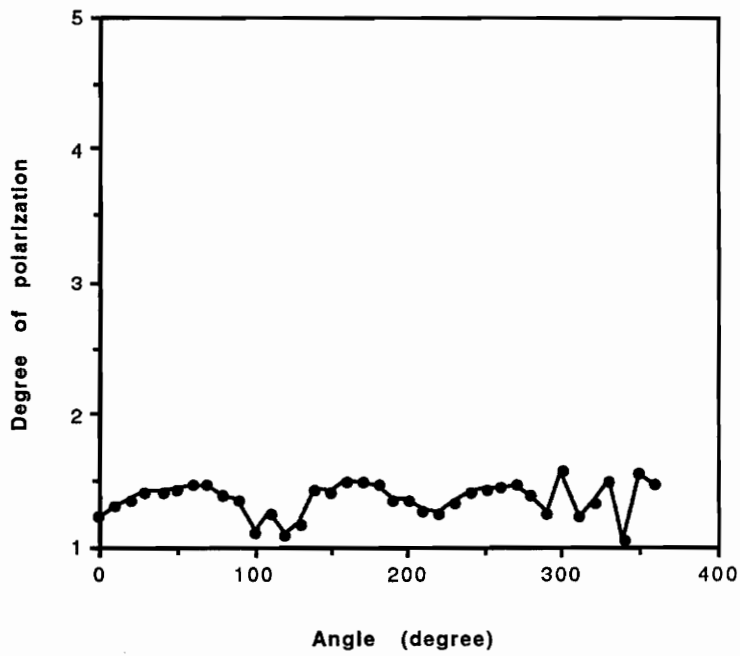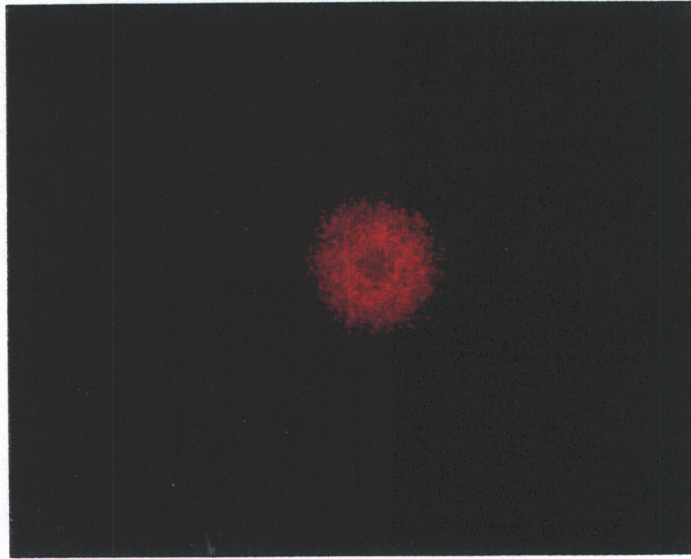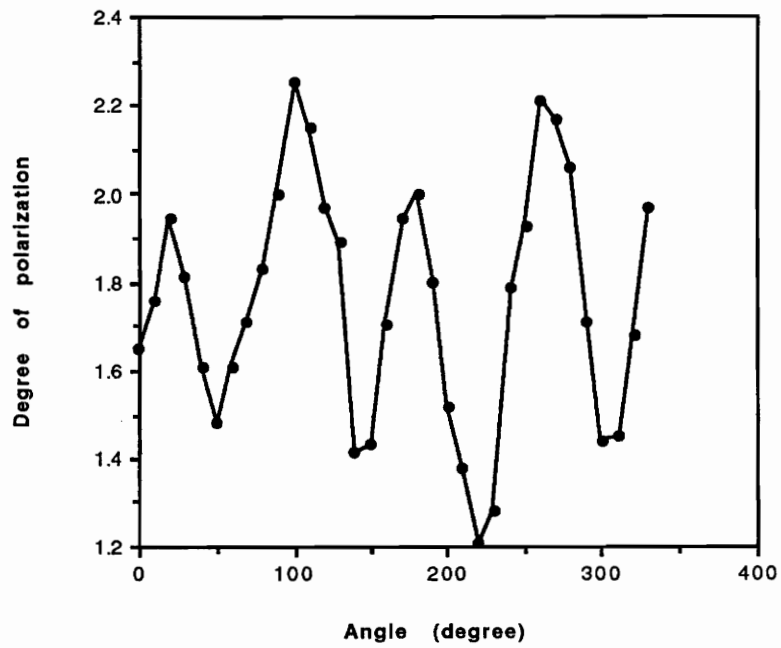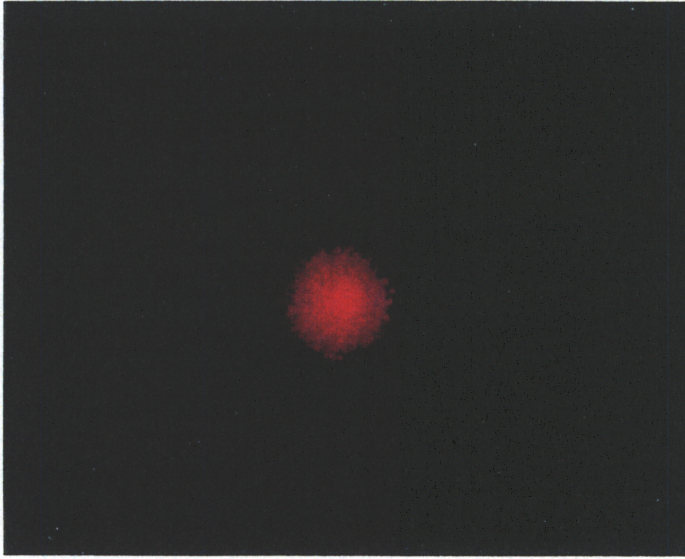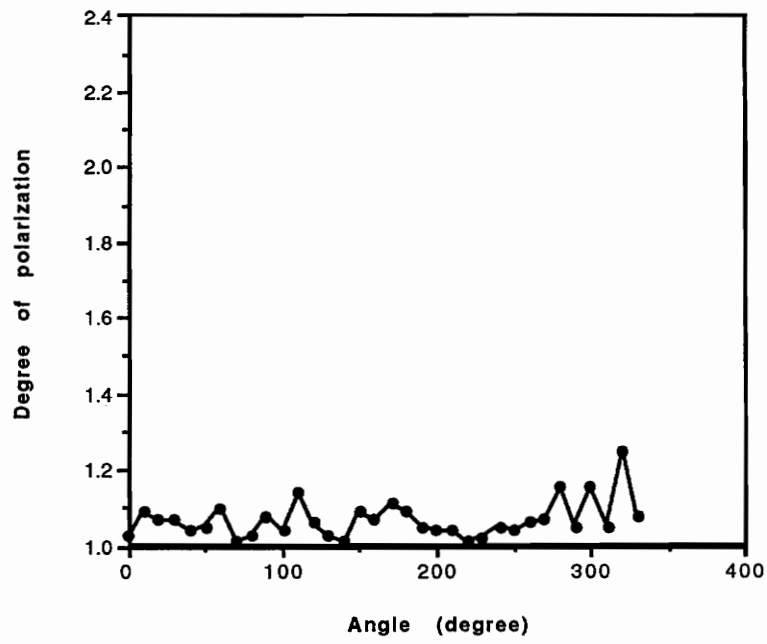
(sapphire fiber 32 cm in length)
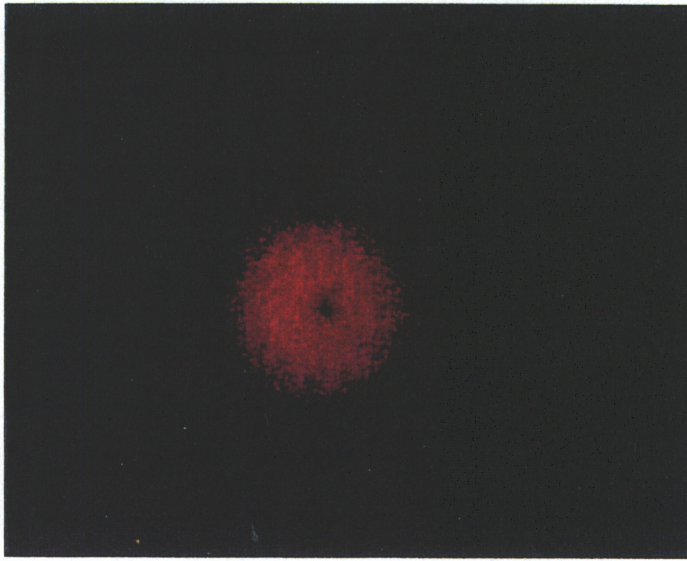
Fig. 4.4.3.3 (b) (2): The field distribution showing sinusoidal variation of

output intensity under the offset launching condition

(sapphire fiber 32 cm in length)

4.4.4 Analyses

The curve showing the periodic sinusoidal variation in Fig. 4.4.3.2 (a) (1) indicates that the single crystal sapphire fiber has partial polarization-maintaining properties when no external effect is applied. The characteristics of polarization-maintaining (PM) sapphire fibers will be described in terms of the following physical parameters: (1) modal birefringence B and beat length L_b, (2) the mode-coupling parameter h and degradation of PM, and (3) transmission loss.

(1) Modal birefringence B and beat length L_b of sapphire fibers

Modal birefringence B is defined as the difference of the refractive index (n_o - n_e) between orthogonal linear-polarization modes, and the B of sapphire fiber is 0.008. The beat length (4.11) is defined as

$$L_b = \lambda / B = 2\pi / \Delta\beta \qquad\qquad (4.4.4.1)$$

where the $\Delta\beta$ is the difference in the propagation constant between the orthogonal modes. The beat length of the sapphire fiber for He-Ne laser light at λ = 632.8 nm is 0.08 mm.

(2) Mode-coupling parameter h and degradation of PM sapphire fibers

There are many factors which degrade polarization-maintenance, expressed as the crosstalk or the mode-coupling parameter.

• Intrinsic factors causing degradation include structural imperfections and the length of the sapphire fiber. These factors are demonstrated by comparison of Fig. 4.4.3.2 (a) (1) and

---

Fig. 4.4.3.3.(a) (1).

• Extrinsic factors causing degradation include temperature, and mechanical perturbations such as bend and twist. These factor effects will be demonstrated in another experiment described later.

• An interesting phenomenon which degraded the polarization-maintenance of sapphire fibers in our experiment was the offset launching condition. With the on-axis launching condition, the field distribution before the analyzer was essentially a uniform pattern with stronger intensity in the middle area, and the resulting curve obtained had a good periodic sinusoidal variation. However, the offset launching condition, as mentioned, produced a donut-like pattern and the poor curve. The reason for this degradation can be explained as follows:

Analyses of the field distribution

Sapphire fibers are not weakly guiding waveguides as they have no cladding. However, they can be treated as weakly guiding waveguides approximately (4.12). Instead of discussing mode theory in circular optical fibers, let us first examine the appearance of modal fields in a planar dielectric slab waveguide (shown in Fig. 4.4.4.1). A cross-sectional view of the slab waveguide looks the same as the cross-sectional view of an optical fiber cut along its axis. The figure shows the field patterns of several of the lower-order modes, which are the solutions of Maxwell's equations of the slab waveguide (4.13-4.16). The order of a mode is equal to the number of field zeros across the guide. The order of the mode is also related to the angle that the ray congruence corresponding to this mode makes with the plane of the waveguide (or the axis of a fiber); that is, the steeper the angle, the higher the order of the mode. The plots show that the electric field of the guided modes is not completely confined to the central dielectric slab (that is, they do not go to zero at the guide-cladding interface), instead, they extend partially into the

cladding. For low-order modes the fields are tightly concentrated near the center of the slab (or the axis of the fiber) with little penetration into the cladding region. On the other hand, for high order modes the fields are distributed more toward the edges of the guide and penetrate further into the cladding region.

In our experiment, when the input linearly polarized light was in-line to the propagating axis of the sapphire fiber, the rays of lower-order modes were parallel to the axis (shown in fig. 4.4.4.2), and the field was concentrated to the axis or the center of the distribution pattern. However, the rays of higher-order modes made larger angles with respect to the axis, and the field was distributed around the center of the pattern symmetrically. The whole intensity distribution for the on-axis launching condition was uniform with strong intensity in the center, as shown in Fig.4.4.3.2 (a) (2). On the other hand, when the input light was offset with respect to the fiber axis, only partially inclined rays (which represent the higher-order modes) could impinge on the fiber (indicated in Fig. 4.4.4.3), and the fields were distributed around the center. But the rays of lower-order modes could not penetrate the sapphire fiber, and the field had no distribution at its center. The whole intensity distribution for the offset launching condition was donut-like pattern, as shown in Fig. 4.4.3.2 (b) (2).

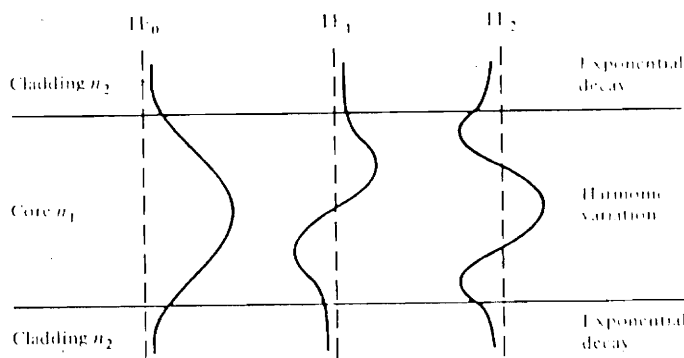Fig. 4.4.4.1: Electric field distributions of the lower-order

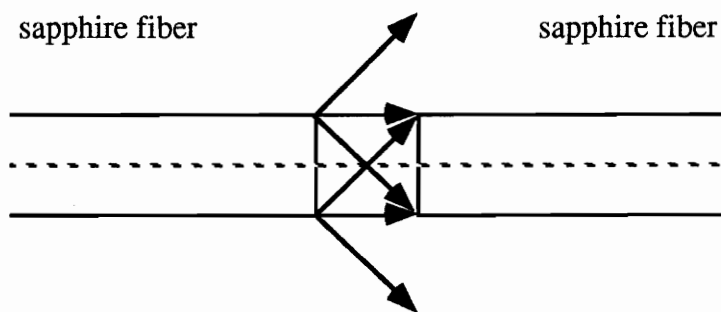modes in a symmetrical-slab waveguide

sapphire fiber

sapphire fiber

Figure 4.4.4.2: On-axis launching condition
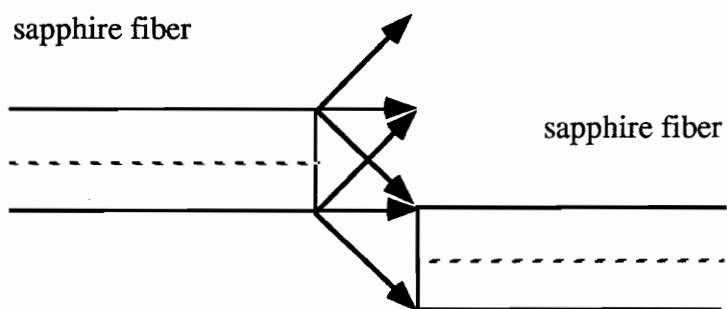
sapphire fiber

sapphire fiber

Figure 4.4.4.3: Off-axis launching condition

Analyses of the qualities of sinusoidal variation curves

It is known that degradation of PM is caused by mode-coupling in the PM fibers. From experimental results of the crosstalk measurand for several kinds of PM fibers using a modified Twyman-Green interferometer (4.12), the following empirical equation can be developed:

$$h = h_0 / (1 + (\Delta \beta L)^2)$$ (4.4.4.2)

where h_0 is a constant, $\Delta \beta$ is the difference in the propagation constants between two modes, and L is the length of the fiber. This relation indicates that the mode coupling parameter is inversely proportional to both the difference in propagation constants ($\Delta \beta$) between the two modes and also to the length of the fiber. According to waveguide theory, $\Delta \beta$ of higher-order modes is much smaller than the lower-order modes, as shown in Fig. 4.4.4.4 (or Fig. 4.4.4.5). Then the intermodal power coupling (or degradation of PM) of the higher-order modes is much stronger than the lower-order modes, and only lower-order modes can show PM properties. Thus the variation in the sine-like behavior of output intensity for different launching conditions can be easily explained by mode coupling theory. As only the lower-order modes posses PM properties, the most sine-like curves are produced when the launching condition is on-axis. On the other hand, when the launching condition is off-axis, the lower- order modes represented by the rays parallel to the axis of the fiber can not pass through the fiber; conversely, the high-order modes represented by oblique light rays can pass through, thereby resulting is a poor sine-shaped curve. The PM properties of higher-order modes have been degraded.

Fig. 4.4.4.4: Plots of the propagation constant (in terms of β/k) as

a function of V for a few of the lowest-order modes

Fig.4.4.4.5: Plots of the propagation constant b as a function of V for LP_{jm} modes

• The polarization of sapphire fibers is partially maintained when a lateral stress is applied to the fiber along or at an angle θ with respect to the principal axis of the fiber. The setup cross sections are shown in Fig. 4.4.4.6, and the corresponding output intensity variation curves are given in Fig. 4.4.4.7. However, external forces such as bend and twist tend to alter the polarization-maintaining properties of sapphire fibers, and the periodic sinusoidal curve is severely degraded, as shown in Fig. 4.4.4.8. The reason is that the energy is coupled between the orthogonally polarized higher-order modes and evanesces from the bare core of the sapphire fiber into the air.
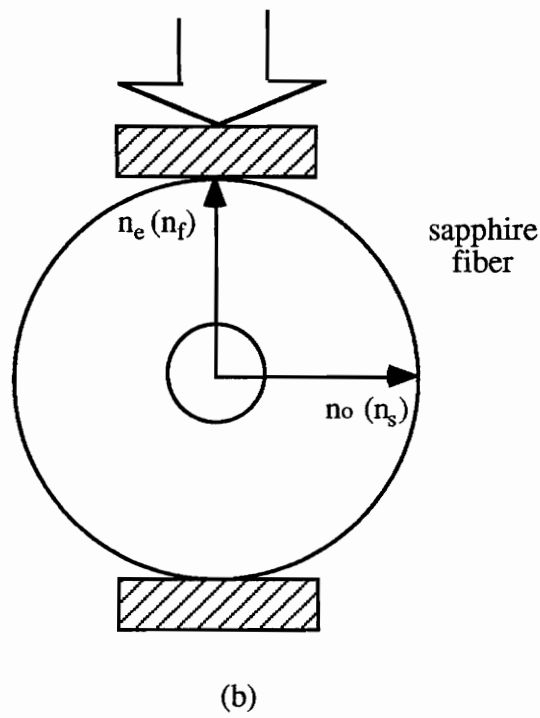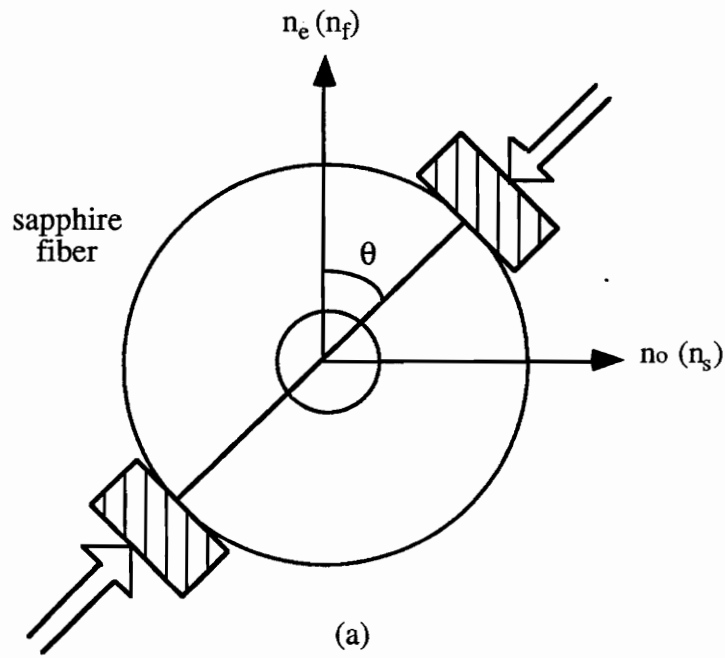
Figure 4.4.4.6: A lateral tress is applied to the sapphire fiber
(a) at an angle θ
(b) along the fast or slow axis of the fiber

Figure 4.4.4.7
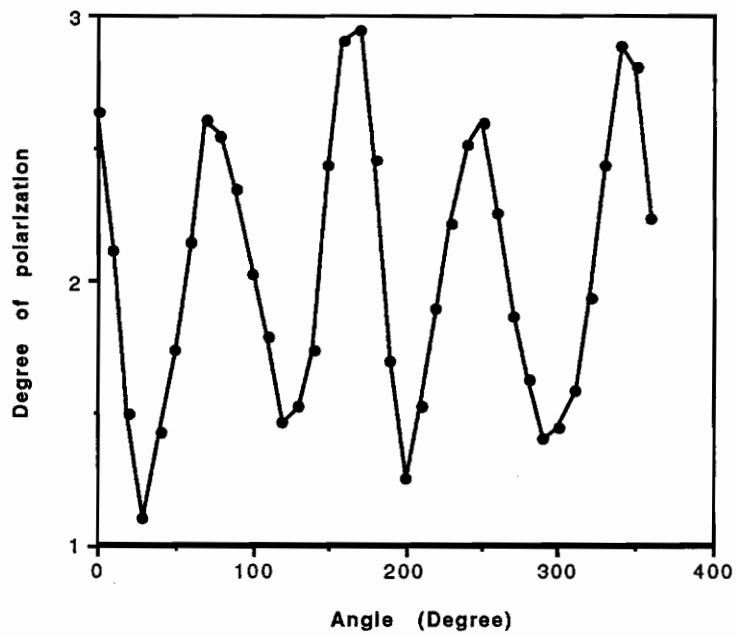
F.g. 4.4.4.7: The sinusoidal variation of the output intensity when a lateral stress

is applied along or at an angle θ with the axis of the sapphire fiber

Figure   4.4.4.8
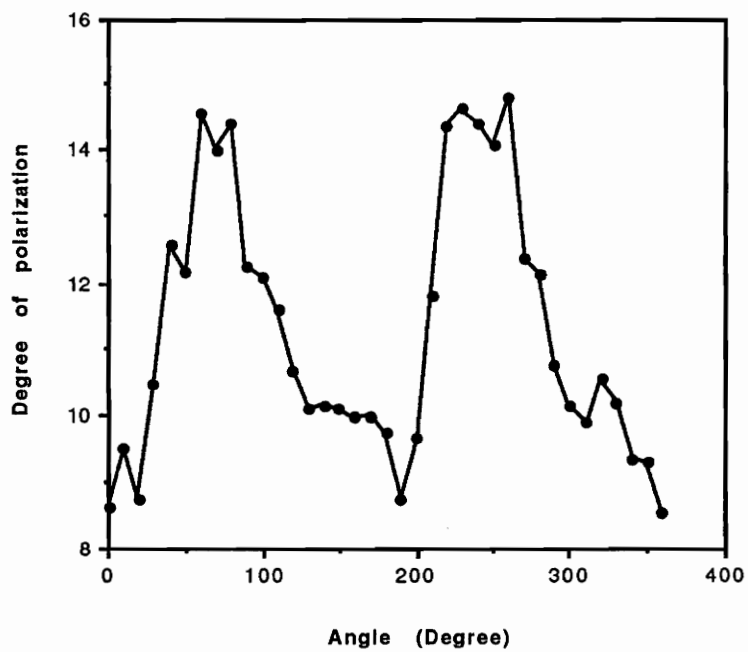
Fig. 4.4.4.8: The severely degraded sinusoidal variation of the output intensity when
an external effect such as bend or twist is applied on the sapphire fiber

(3) Transmission losses

The amount of transmission loss depends on the birefringence of the fibers. The optical losses of sapphire fibers are large, one reason being that the B (8×10^{-3}) of sapphire is higher than of other fibers. There is no definite classification separating the low birefringence (LB) and high birefringence (HB) fibers (4.17), but it is generally agreed that the birefringence of LB and HB is between 10^{-6} to 10^{-4}. So, in applications of sapphire sensors, the sensor head of sapphire fiber is usually chosen to be less than 15 cm.

4.4.5 Conclusion

The polarimetric analyses of the experiments done with single crystal sapphire fibers demonstrate that sapphire fibers have polarization-maintaining properties. Further, launching conditions reveal that only lower-order modes of multimode sapphire fibers can preserve the state of linear polarization, or stated equivalently, the polarization-maintaining ability (PMA) is dependent on the mode-coupling parameter. The PMA is 6 dB for 7 cm and 3 dB for 32 cm long tested sapphire fibers. Based on the polarization-maintaining properties and temperature dependence of the phase delay ($\delta = 2\pi \Delta n L / \lambda$), a polarimetric phase sensor for high temperatures was designed.

4.5 The Polarimetric Optical Sensor of the Birefringent Single Crystal Sapphire Fiber for High Temperature Measurements

4.5.1 Introduction

Polarimetric fiber sensors have been employed for measurements of electric current, voltage, pressure, acceleration, and liquid level for many years (4.18-23). As the optical material of these sensors can not withstand high temperature, they can only be used in low-temperature applications. The increasing requirement of high-temperature applications has made researchers investigate the birefringent single crystal sapphire fiber as a sensor for high-temperature measurements, owing to its high melting point of 2040° C. The previous experiments have demonstrated the polarization-maintaining properties of birefringent single crystal sapphire fibers at room temperature, and it will be shown in the next section that partial polarization-preservation at high temperatures over 1000 °C is possible under the proper launching condition. In addition, a polarimetric sapphire fiber sensor based on the polarization - maintaining properties and the temperature dependence of phase delay $\delta = 2\pi \, \Delta nL / \lambda$ is described.

4.5.2 Experimental Setup

For high-temperature measurements the experimental setup of the polarimetric optical sensor is similar to that of the polarimetric analyses of birefringent sapphire fibers, as

shown in Fig. 4.5.2.1. The difference in these two experiments is in the sensing parts. Three pieces of sapphire fibers constituting this sensor are sandwiched between a polarizer and an analyzer orthogonal to the former. The middle piece of the sensor is a sensing fiber, 1.4 cm long and 97 μm in diameter. The first and the third pieces of the sensor act as lead-in and lead-out fibers with the principal axes rotated parallel (or orthogonal) to the transmission axis of the polarizer P_1. The advantage of this design of lead-in and lead-out sapphire fibers is that it prevents the polarizer and analyzer from becoming heated. The connection between the ends of the middle sensing fiber and the first fiber, 10 cm long and 100 μm in diameter, is achieved by using a small piece of a sapphire hollow tube, 100 μm in diameter, to confine the two fibers. Similarly, the connection between the ends of the middle and the third fiber, 3 cm long and 97 μm in diameter, is achieved through another small piece of sapphire tube with a diameter of 100 μm. The three pieces of sapphire fibers are connected end to end in such a way that the principal (slow or fast) axis of the middle sensing fiber is oriented at 45° with respect to the principal axis of the lead-in and lead-out sapphire fibers, which are aligned parallel (or orthogonal) to the transmission axis of the polarizer P_1 separately, as shown in Fig. 4.5.2.2. A chamber is used to provide uniform temperature changes in the middle sensing fiber as heating is obtained using a torch.
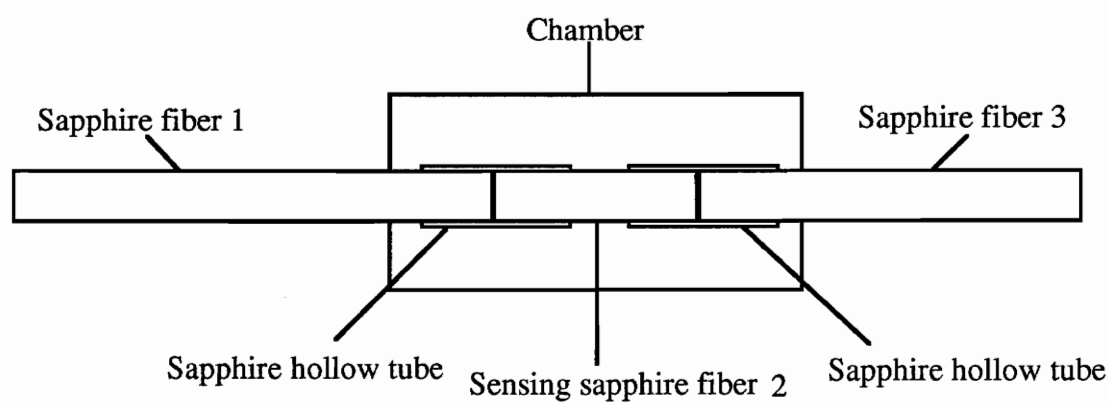
Enlarged view of sensing sapphire fiber
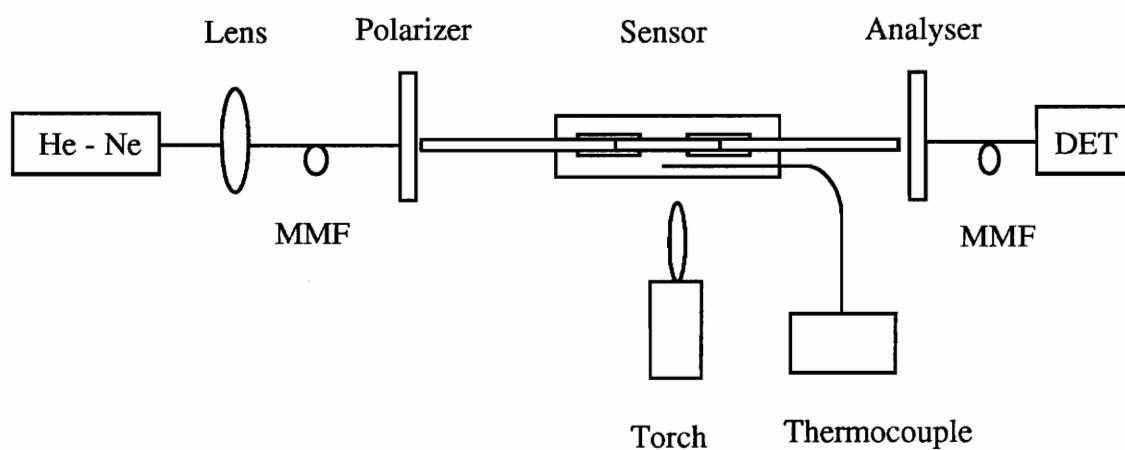
Figure 4.5.2.1: The setup of sapphire fiber sensor for high temperatures
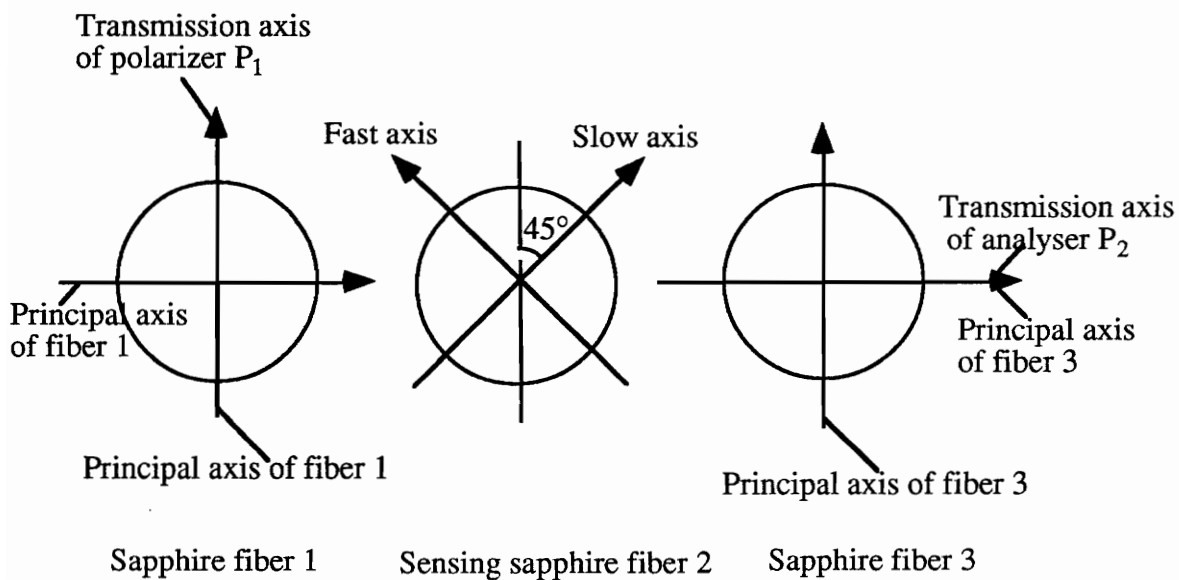
Figure 4.5.2.2: Orientation of three pieces of sapphire fiber

4.5.3 Processing and Results

After passing through the polarizer P_1, the light became linearly polarized. A state of linear polarization was maintained after launching along the principal axis of the lead-in sapphire fiber 1. On the front face of the middle sensing fiber 2, the linearly polarized light was decomposed into two orthogonal components along the fast and slow axes of the sensing fiber separately. After passing through the sensing fiber, the output components were decomposed again on the principal axis of the lead - out sapphire fiber 3,

which was parallel to the transmission axis of the analyzer P_2. The plot of the decomposition is shown in Fig. 4.5.3.1. The output intensity is represented by

$$\begin{aligned} I_{out} &= E_0{}^2 \sin^2 2\theta \, \sin^2 (\delta/2) \\ &= 4 \, E_0{}^2 \, \cos^4 (45°) \sin^2 (\pi \, \Delta n \, L_2 / \lambda) \\ &= E_0{}^2 \sin^2 (\pi \, \Delta n \, L_2 / \lambda) \end{aligned} \qquad (4.5.3.1)$$

where $\theta = 45°$, L_2 is the length of the sensing fiber, and $\delta = (2\pi \, \Delta n \, L_2 / \lambda)$ is the phase difference of the two coherent components, $E_0 \sin 45° \cos 45°$ and $E_0 \cos^2 45°$.
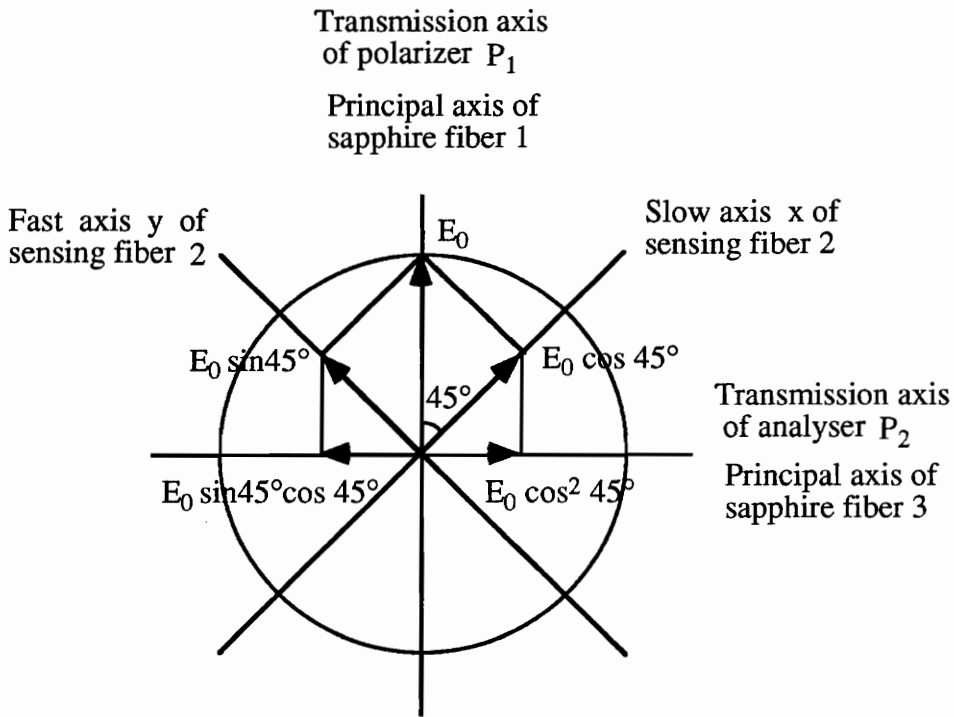

Figure 4.5.3.1: Decomposition of the input linearly polarized light

As the optical path difference ΔnL is a function of temperature, the output intensity is a sine squared function of the temperature. When the argument $\delta/2$ (or the phase δ) of the function changes from 0 to π (or 2π) radians the output power will periodically vary from a minimum to a maximum and back to a minimum value. In order for the sensing technique to be usable the argument $\delta/2$ (or phase δ) of the sine-squared function can not change by more than $\pi/4$ (or $\pi/2$) radians. In our experiment, since the length of the middle sensing fiber L_2 was chosen as 1.4 cm, the birefringence Δn was 0.008, and the wavelength λ of the He-Ne laser was 0.6328 μm, the phase δ was approximately $(35+1/2)\pi$. When the temperature varied from 25 °C to around 1000 °C, δ changed approximately $\pi/2$, as shown in Fig. 4.5.3.2. Figure 4.5.3.3 shows a comparison between the experimental intensity variation and the theoretical sinusoidal intensity variation with respect to temperature. It is noted that they are matched so well that the experimental output intensity is almost a sinusoidal variation, and the empirical temperature coefficient measured is not sensitive to temperature as it is only 0.0208 rad. / °C m. This demonstrates that the linear polarization is still maintained partially at high temperatures as the sinusoidal variation of the output intensity is the result of polarization interference which is a sine squared function of temperature. This property of sapphire fiber has already been mentioned in Chapter 3.
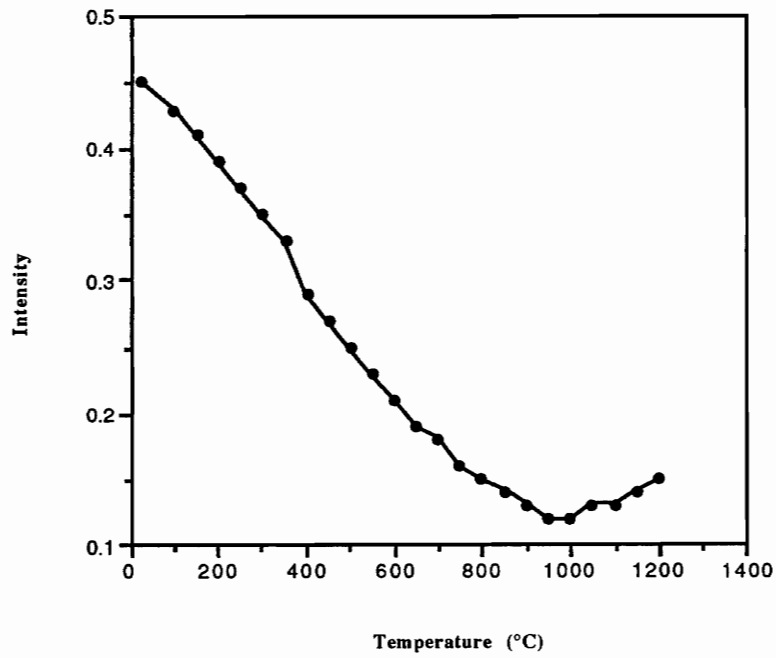
Figure   4.5.3.2

Fig.4.5.3.2: Empirical output intensity variation

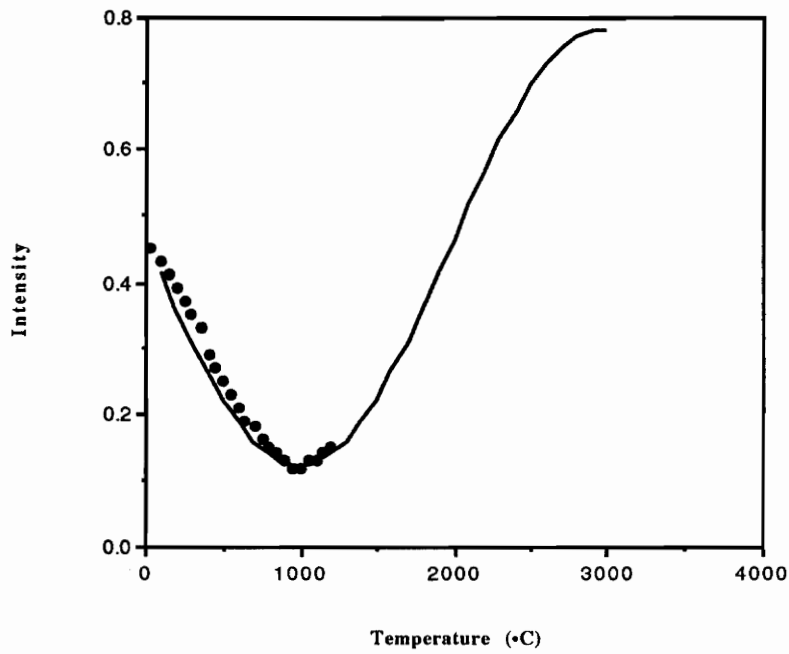with respect to temperature

Figure 4.5.3.3

Fig.4.5.3.3: Comparison between empirical output intensity

variation and theoretical sinusoidal intensity

variation with respect to temperature

3.3.3.4.5.4 *Conclusion*

The design of a polarimetric sapphire fiber sensor for high temperature measurements is based on the properties of withstanding high temperatures, polarization preservation and temperature dependence of phase delay. According to experiments conducted, the linear polarization of sapphire fibers is partially maintained at both room and high temperatures; or stated equivalently, the birefringence (B = Δn) of sapphire fibers is not sensitive to temperature. The temperature coefficient of sapphire fibers has been found to be 0.0208 rad / °C m. A resolution of 2 °C has been obtained over the measurement range of 25 °C to 800 °C. This sensor can be operated at temperature above 1500 °C. The polarization-maintaining ability (PMA) is 6 dB and 3 dB for tested sapphire fibers 7 cm and 32 cm long, respectively. It is also observed that the PMA is strongly dependent on the mode-coupling parameter. As the temperature dependence of phase delay ($\delta = 2\pi \Delta nL / \lambda$) is proportional to the fiber length (L) and the birefringence (B = Δn) which is not sensitive to the temperature, a strain sensor operated at high temperatures is worth additional study.

Chapter 5 - Conclusions and Future Direction

Birefringent single crystal sapphire fibers have many advantages for optical fiber sensors:

• special properties such as chemical resistance, bio-inertness and nontoxicity have made sapphire fibers useful in a corrosive environment,

• the high temperature melting point of 2040 °C enables sapphire fibers to be used in high temperature measurements, and

• polarization-maintaining properties enable sapphire fibers to be used in polarimetric phase interferometers as a good sensitive sensors.

Based on its properties of withstanding high temperatures, polarization preservation, and temperature dependence of phase delay, a polarimetric sapphire fiber sensor for high temperature measurements has been designed. Experimental results have indicated that the polarization-maintaining ability (PMA) is 6 dB and 3 dB for 7 cm and 32 cm long sapphire fibers, respectively. Meanwhile, it is observed that the PMA of sapphire fibers is strongly depended on the mode-coupling parameter. The temperature coefficient of the different phase delays between the orthogonal modes is 0.0208 rad /m °C, and the corresponding resolution is 2 °C over the range of 25 °C to 800 °C. This sensor may be operated at temperatures above 1500 °C. Based on the fact that the phase delay ($\delta = 2\pi \, \Delta nL / \lambda$) is proportional to the sensing fiber length L, and the birefringence ($B = \Delta n$) is not sensitive

to the temperature, a new sensor for strain measurements at high temperatures is expected in the near future.

References

1.1   V. Aschoff, "Optische Nachrichtenubertragung im klassischen Altertum," Nachrichtentechn. Z. (NTZ), vol. 30, pp. 23-28, Jan. 1977.

1.2   H. Busignies, "Communication channels," Sci. Amer., vol. 227, pp. 99-113, Sept. 1972.

1.3   A. B. Carlson, Communication systems, McGraw-hill, New York, 3rd ed., 1986.

1.4   T. H. Maiman, "Stimulated optical radiation in ruby," Nature vol 187, pp. 493-494, Aug. 1960.

2.1   Eugene Hecht, "Optics", p. 334-336.

3.1   G. A. Magel, D. H. Jundt, M. M. Fejer, and R. L. Byer, "Low-loss single-crystal sapphire optical fibers", Proc.SPIE, vol. 618, p. 89, 1986.

3.2   Bomstein, Zahlenwerte und Funktionen, sechste Auflage, Springer Verlag, Vol. 2, (1971).

3.3   K. I. White, "A calorimetric method for the measurement of low optical absorption losses in optical communication fibers", Optical and Quantum Electronics 8, 73 (1976).

3.4   T. J. Turner and J. H. Crawford, Jr, "V centers in single crystal Al2 O3", Solid State Commun. 17, 167 (1975).

3.5   D. Jundt, M. Fejer, R. Byer, "Growth and optical properties of single-crystal sapphire fibers", Proc. SPIE, vol. 1048, p. 39, 1988.

3.6   D. P. Dover, R. C. Paster, and L. G. Deshazer, "Hydroxyl impurity effects in YAG (Y3 Al5 O12)", J. Chem. Phys, 4104 (1984).

3.7   R. S. Feigelson, W. L. Kway and R. K. Route, "Single crystal fibers by the laser

heated pedestal growth method", Proc. SPIE, vol. 484, p. 133, 1984.

3.8 S. Musikant, Optical Materials, an Introduction to Selection and Application, Marcel Dekker, Inc., New York, 1985.

3.9   B.Bendow, H. Rast and O. H. El-Bayoumi, "Overview of infrared fibers: prospective materials, fabrication methods and applications", Proc. SPIE, vol. 505, p. 151, 1984.

3.10   D. Dianov, L. Dmitruk and V. Plotnichenko, "Two layer single crystal fibers grown by Stepanov's method", Proc. SPIE, vol. 799, p. 84, 1987.

3.11   G. N. Merberg and J. A. Harrington, "Optical and mechanical properties of single crystal sapphire optical fibers", Applied Optics, vol. 32, No. 18, 1993.

3.12   J. Gilman, The Art and Science of Growing Crystals, John Wiley and Sons, Inc., New York, 1963.

3.13   B. Pamplin, Crystal Growth, Pergammon Press, New York, 1966.

3.14 C. A. Burrus and L. A. Coldren, "Growgth of single crystal sapphire clad ruby fibers," Appl. Phys. Lett. 31, 383-384 (1977)

4.1   I. P. kaminow, "Polarization in Optical Fibers", IEEE J. Quant. Elec., vol. QE-17, No. 1, 1981.

4.2 D. chardon and S. J. huard, "A New Interferometric and Polarimetric Temperature Optical Fiber Sensor", J. Lightwave Tech. vol. Lt-4, p. 720-725, 1986.

4.3   D. N. payne, A. J. barlow, and J. ramskov hansen, "Development of Low- and High-Birefringence Optical Fibers", IEEE J. Quan. Elec., vol. QE-18, p. 477-487, 1982.

4.4 W. Eickhoff, "Temperature sensing by mode-mode interference in birefringent optical fibers", Opt. Lett. vol. 6, pp. 204-207, 1981.

4.5   R. Ulrich and M. Johnson, "Fiber-ring interferometer: Polarization analysis", Opt. Lett., vol. 4, pp. 152-154, 1979.

4.6   S. K. Sheem and T. G. Giallorenzi, "Polarization effects on single mode optical fiber sensors", Appl. Phys. Lett. vol. 35, pp. 914-917, 1979.

4.7   V. Ramaswamy, W. G. Frech, and R. D. Standly, "Polarization characteristics of noncircular core single-mode fibers", Appl. Opt., vol. 17, pp. 3014-3017, 1978.

4.8   R. Ulrich and A. Simon, "Polarization Optics of twisted single-mode fibers", Appl. Opt. vol. 18, pp. 2241-2251, 1979.

4.9   J. Sakai and T. Kimura, " Birefringence and polarization characteristics of single-mode optical fibers under elastic deformations:, IEEE J.Quan. Elec., vol. QE-17, pp. 1041-1051, 1981.

4.10   R. H. Stolen, V. Ramaswamy, P. Kaiser, and W. Pleibel, "Linear polarization in birefringent single-mode fibers", Appl. Phys. Lett., vol. 33, pp. 699-701, 1978.

4.11   J. noda, K.okamoto, and Y. sasaki, "Polarization-Maintaining Fibers and Their Applications", J. Lightwave Technol., vol. LT-4, p. 1071-1089, 1986.

4.12   K. Tsubokawa, N. Shibata, and S. Seikai, "Evaluation of polarization-mode coupling coefficient from measurement of polarization-mode dispersion," J. lightwave Technol. vol. LT-3, no. 4, pp. 850-854, 1985.

4.13   G. Keiser, "Optical Fiber Communications".

4.14   D. Marcuse, "Theory of Dielectric Optical Waveguides", Academic, New York, 1974.

4.15   J. Midwinter, "Optical Fibers for Transmission", Wiley, New York, 1979.

4.16   R. L. Gallawa, "A User's Manual for Optical Waveguide Communications", publication no. OTR76-83, U.S. Dept. of Commerce, Washington, DC, 1976.

4.17   H. G. Unger, "Planar Optical Waveguides and Fibers", Clarendon, Oxford, 1977.

4.18   J. noda, K.okamoto, and Y. sasaki, "Polarization-Maintaining Fibers and Their Applications", J. Lightwave Technol. , vol. LT-4, p. 1072, 1986.

4.19   A. Papp, and H. Harms, Appl. Opt. 19, 3729 (1980).

4.20   T. Mitsui, K. Hosoe, H. Usami, and S. Miyamoto, IEEE Trans. Power Del. PWRD-2, 87 (1987).

4.21   W. B. Spillmam, Jr., Opt. Lett. 7,388 (1982).

4.22   S. Tai, K. Kyuma, and M. Nunoshita, Appl. Opt. 22, 1771 (1983).

4.23   A. Wang, Z. Liu, B. Wu, S. He, H. Qi, J. Yao, and J. Lin, presented at Fourth International Conference on Optical Fiber Sensors, Tokyo, 1986.

Vita

The author was born on April 29, 1946 in Hebei Province, China. In 1970 she graduated from Tianjin Normal University, Tianjin, China. She had worked in the same University as a lecturer and researcher for many years. She came to America as a visiting scholar in 1987 and had worked in Towson State University of Maryland and Virginia Polytechnic Institute and State University for two years. In 1991 she enrolled at the Virginia Polytechnic Institute and State University's Graduate School program in the Department of Electrical Engineering. She has been working as a graduate research assistant under Professor R. O. Claus at the Fiber and Electro-Optics Research Center since 1992.

Her research interests include optical fiber sensors, communications, laser technology, and applications of holography.